Journal of Structural Geology 173 (2023) 104895

Contents lists available at ScienceDirect

Journal of Structural Geology

journal homepage: www.elsevier.com/locate/jsg

Geochemistry of syntaxial calcite veins in ultra-deep sandstone reservoirs from the Kuqa depression, western China

Shunyu Wang [a], Keyu Liu [a,b,*], Jian Wang [a,**], Yong Li [c], Zhenkun Li [a], Haijun Yang [c], Tao Mo [c]

[a] School of Geosciences, China University of Petroleum, Qingdao, Shandong, 266580, China
[b] Laoshan Laboratory, Qingdao, 266071, China
[c] Tarim Oilfield Company, PetroChina, Korla, Xinjiang, 841000, China

ARTICLE INFO

Keywords:
Syntaxial veins
Fluid evolution
In situ geochemical analysis
Ultra-deep reservoirs
Kuqa depression

ABSTRACT

Extensional fractures filled with calcite are widespread in the ultra-deep reservoir sandstones of the Cretaceous Bashijiqike Formation (>6000 m) in the Kuqa Depression, western China. Microstructures of calcite veins provide an excellent opportunity for investigating fracture opening processes in a tectonically active, ultra-deep foreland basin setting. The syntaxial calcite vein is the dominant type and is formed through a single crack-seal event. Calcite crystals in fractures show blocky and elongated blocky shapes. The textural and geochemical characteristics of syntaxial calcite veins were investigated in detail using optical cathodoluminescence, trace element distributions and stable carbon and oxygen isotopes. Calcite veins were inferred to have precipitated from a mixture of seawater and meteoric water. $\sum$REE + Y and elemental concentrations of Mg^{2+}, Mn^{2+}, Fe^{2+} and Sr^{2+} both increase from fracture walls to the center. This process was controlled by temperature, crystal growth rate and variations in elemental concentration in a relatively closed environment. Medium REE-bulge patterns after Post Archean Average Shale (PAAS) normalization, negative δCe and positive δEu anomalies all indicate that calcite wall-rock cements and veins may inherit constituents from seawater and from meteoric water containing feldspar-weathering components, respectively. Both $^{13}\delta C_{PDB}$ and $^{18}\delta O_{SMOW}$ of the parent fluids imply that calcite veins were primarily precipitated from seawater under a relatively closed diagenetic environment. Considering the scope and timing of the transgression of the Tethyan Ocean in the study area, meteoric water may have been retained prior to the seawater invasion (65 Ma). The mixing of meteoric water and seawater within the reservoir could be the primary origin of the fluids forming the calcite veins.

1. Introduction

Subsurface fractures and fluid flow can be simultaneously induced by tectonic movements. Consequently, tectonically induced mineral veins (e.g., calcite and quartz) can record fluid flow and diagenetic environment changes. Open fractures are crucial fluid pathways for petroleum migration and mineral deposition in ultra-deep (≥6 km) reservoirs (Solano et al., 2011; Kang et al., 2013; Fall et al., 2015; Lyu et al., 2017; Li et al., 2019; Liu et al., 2021), and oversaturated pore fluids can enter tectonically induced fractures and precipitate mineral veins. As a result, the microstructures and fine-scale geochemical features of these mineral veins can record fluid events (Barker et al., 2006, 2009; Bons et al., 2012; Maskenskaya et al., 2014; Laubach et al., 2019). Delineation of deep-seated fluids is essential for understanding the evolution of ultra-deep reservoirs. In this study, calcite veins from *ca.* 6 km depth are described using petrological and geochemical evidence in order to investigate potential fluid origins and evolution.

Mineral deposits may precipitate during fracture opening or after fractures cease opening (termed syn- and post-kinematic deposits, respectively; Laubach, 1988) and consequently may record conditions existing at different times. Moreover, deposits formed during fracture opening can record a progression of conditions if repetitive fracture opening and sealing is recorded by veins within microstructures. In fractures formed in low-temperature diagenetic environments, crack-seal textures may form bridge cements that span between fracture walls (e.g., Laubach et al., 2004; Hilgers and Urai, 2005; Gale et al., 2010; Lander and Laubach, 2015) leaving space in the fracture for post-kinematic cementation (blocky, textureless etc.) (Laubach, 2003).

* Corresponding author. School of Geosciences, China University of Petroleum, Qingdao, Shandong, 266580, China.
** Corresponding author.
E-mail addresses: liukeyu@upc.edu.cn (K. Liu), wangjian8601@upc.edu.cn (J. Wang).

https://doi.org/10.1016/j.jsg.2023.104895
Received 5 October 2022; Received in revised form 22 May 2023; Accepted 31 May 2023
Available online 7 June 2023

The presence of vein microstructures is generally interpreted as evidence for cyclic changes in fluid pressure and/or far-field stress (Fisher and Brantley, 1992; Fall et al., 2015; Hooker and Katz, 2015; Laubach et al., 2019).

Veins within syn- and/or post-kinematic textures thus provide a record of fluid properties and precipitation conditions when fractures formed. Such deposits may record sequential changes of fluid temperatures, compositions, origins and horizon pressures during rock deformation (Becker et al., 2010; Fall et al., 2015; Laubach et al., 2019). In fractures, mineral veins can show various internal microstructures with different crystal shapes (blocky, fibrous, stretched etc.) and growth directions (e.g., either from the wall rock into the vein or in the opposite direction) (Ramsay, 1983; Passchier, 1996; Bons et al., 2012; Ukar and Laubach, 2016) (Fig. 1).

The focus of this study is an ultra-deep (≥6 km) clastic reservoir, the Cretaceous Bashijiqike Formation (K_{1bs}) in the Kuqa Depression, western China. In the Kuqa foreland thrust belt multiple fractures and carbonate veins were developed (Liu et al., 2009; Zeng et al., 2010; Lai et al., 2017), providing excellent diagenetic records for studying microstructures and geochemical indicators of calcite veins. As is discussed below, the active tectonic setting in which these fractures and veins were formed make it likely that the fractures were a response to tectonic shortening and were fractured mechanically. The principal purpose of this study is to establish the relationship between the microstructures of calcite veins and their associated geochemical characteristics, and to reconstruct fluid evolution during fracture openings. As such, this is the first interdisciplinary investigation of microstructures and geochemical characteristics of tectonic veins in the Bashijiqike Formation of lower Cretaceous, Kuqa Depression. The results provide insights into the coupling of tectonic and diagenetic processes and fluid evolution in a deep burial foreland basin setting.

2. Geological setting

The Kuqa Depression is in the northern part of Tarim Basin western China (Fig. 2 a). The study area, about 220 km long and 30 km wide (Liu et al., 2022), is within the Kelasu Fold Belt, which is rich in oil and gas. From west to east, the Kelasu fold belt is divided into four zones: the Awate, Bozi, Dabei and Keshen zones (Fig. 2 b). Fault-bend traps in the Kelasu Fold Belt are mainly thrusting-related folds (Fig. 2 c), whose development and evolution has been primarily controlled by the Late Yanshan (approximately 65 Ma) and Himalayan (approximately 23.3 Ma) orogenies (Shi et al., 2020; Wang et al., 2021). Although the tectonic evolution stages of the Kuqa Depression are still uncertain (Jia et al., 1998; Chen et al., 2004; Li et al., 2004), the prevailing view is that the Kuqa Depression has experienced continuous deformation since the beginning of the Cenozoic (Yin et al., 1998; Chen et al., 2004, 2005; Jin et al., 2008). During the late Cretaceous, the entire Kuqa Depression was uplifted and the upper part of the Cretaceous horizon began to be eroded (Fig. 3). Subsequent to the deposition of the Kuqa Formation in the Neogene and Quaternary, the collision between the Indian Plate and the Eurasian Plate has led to more intensive shortening and massive thrust-nappe structures (Graham et al., 1993; Lu et al., 1994; Yin et al., 1998; Chen et al., 2004; Boorder, 2012).

The Cretaceous Bashijiqike Formation (K_{1bs}) is a major hydrocarbon reservoir in the Kuqa Depression (Lai et al., 2017, 2021; Shi et al., 2020; Wang et al., 2021) with burial depths varying from 3 to 8 km (Fig. 3 a) (Chen et al., 2000; Zou et al., 2006; Shi et al., 2020). The predominantly terrestrial sediments are mainly derived from the southern Tianshan Orogenic Belt (Ma et al., 2016) (Fig. 2 b). Since the early Cretaceous, the region has evolved from a warm, moist to an arid, hot climate (Jiang et al., 2007; Li et al., 2013), and K_{1bs} was deposited in the early Cretaceous in a fluvial-fresh-water lacustrine deltaic setting (Guo et al., 2002). Feldspathic lithic sandstone and lithic feldspar sandstones are widespread within the lacustrine delta depositional systems, which are controlled by braided rivers (Zeng et al., 2010; Wang et al., 2021). The remnant thickness of K_{1bs} is approximately 100–360 m. During the late Cretaceous, the Tethys Ocean flooded the region from west to east and submerged the remnant K_{1bs} in the Kuqa Depression (Guo et al., 2002), providing highly oxidizing seawater as a major fluid type for mineral deposition during this period.

3. Materials and methods

Opening-mode fractures and carbonate veins were developed in the Dabei and Keshen Zones in drilling cores (Fig. 4) (Zhang et al., 2020; Lai et al., 2021; Wang et al., 2021). Various fracture-filling minerals were found in the studied area, including carbonate cement (calcite, dolomite and ankerite) (Figs. 4 and 5) and euhedral quartz (Fig. 5 f-i). Rock samples from 15 wells were stained with a mixed solution of Alizarin Red S and K-ferricyanide to distinguish carbonate mineral types (Dickson, 1966; Finkelman and Lindholm, 1972).

In order to obtain *in situ* analysis of elemental concentrations in various parts of carbonate cement, total of 50 points of the same thin sections from two calcite veins were used to conduct optical cathodoluminescence (CL), Electron Microprobe Micro-Analysis (EMPA) and Laser Ablation Inductively Coupled Plasma Mass Spectrometry (LA-ICP-MS). Powdered calcite samples from 13 calcite veins and 20 wall rocks

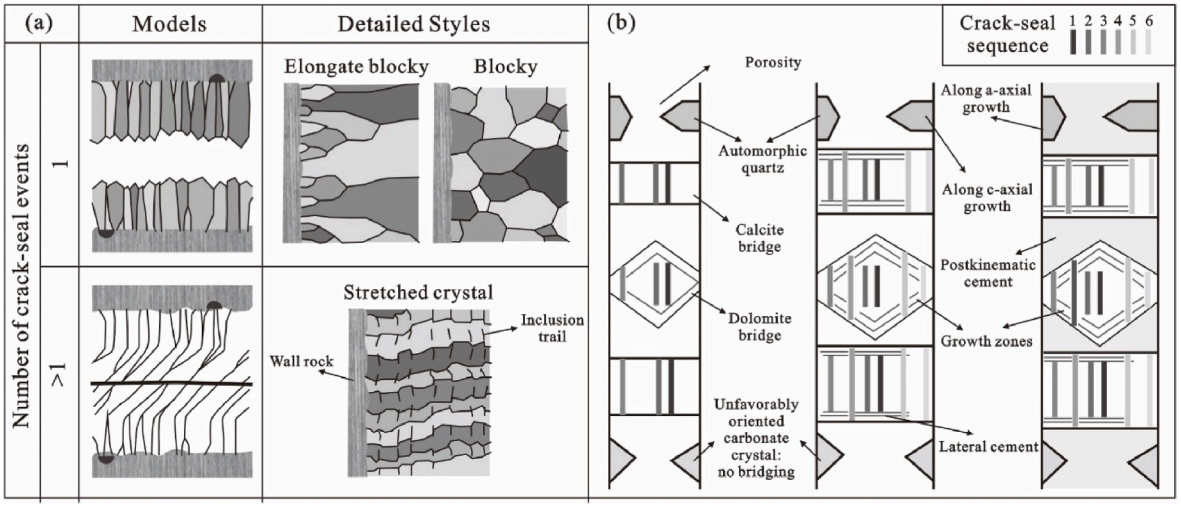

Fig. 1. (a) Basic scheme of internal crystal morphology within syntaxial veins that have experienced single or multiple crack-seal events (Bons et al., 2012). (b) Basic scheme depicting growth of syn- and post-kinematic crystals during fracture opening (after Ukar and Laubach, 2016).

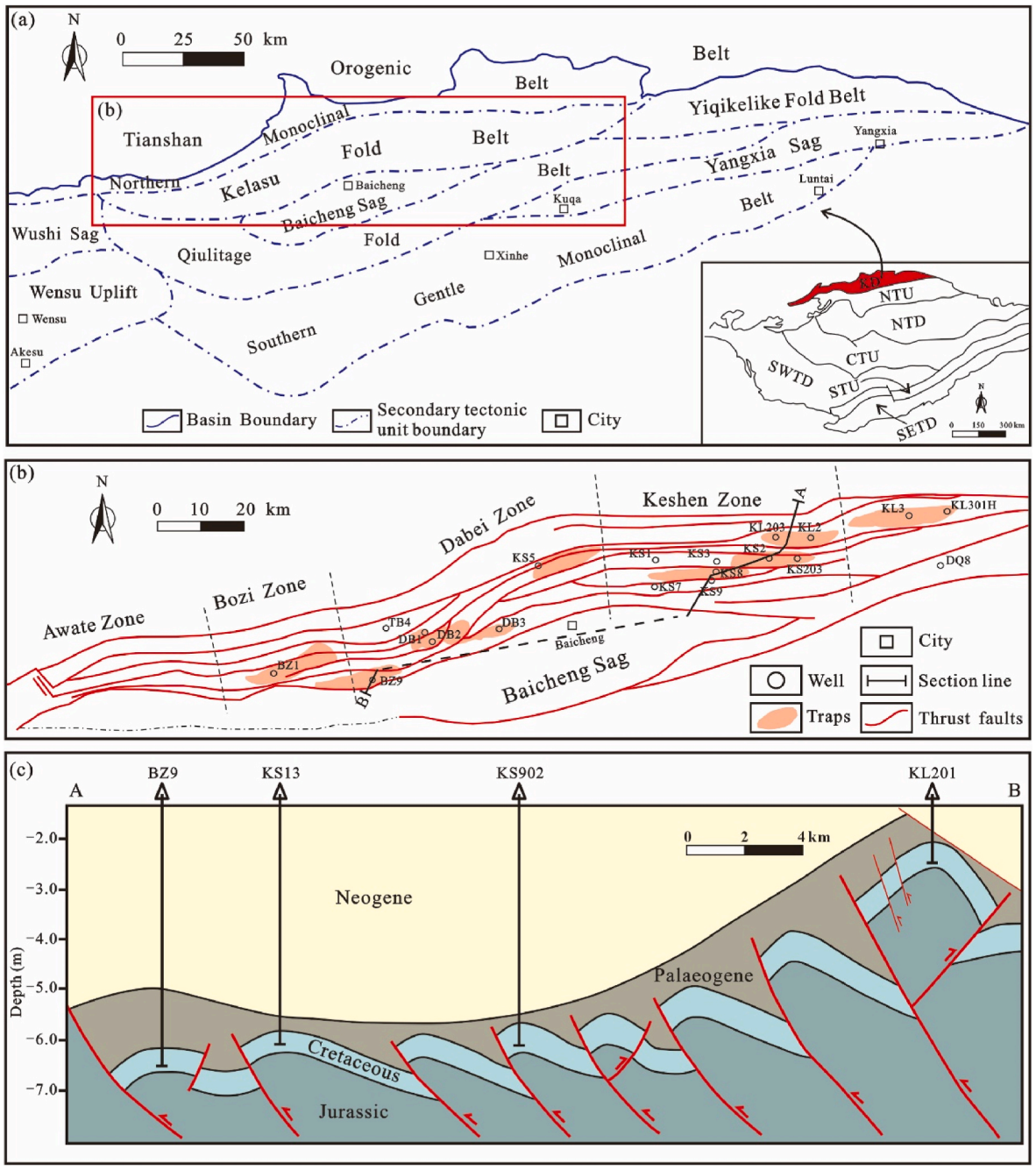

Fig. 2. (a) Geographic location of the Kelasu Thrust Belt and subdivisions of structural elements in the Kuqa Depression, Tarim Basin (after Yu et al., 2016; Lai et al., 2021; Wang et al., 2021). KD - Kuqa Depression; NTU - North Tarim Uplift; NTD - North Tarim Depression; CTU - Central Tarim Uplift; SWTD - Southwest Tarim Depression; STU - South Tarim Uplift; SETD - Southeast Tarim Depression. (b) Enlarged map of the Kelasu Thrust Belt and mapping locations of four zones (from west to east: Awate, Bozi, Dabei and Keshen) (after Lai et al., 2017, 2021; Wang et al., 2021); (c) Representative geological profile perpendicular to the local structural trend. The profile location (A–B) is marked in Fig. 2 (b) (after Lai et al., 2021).

were used for stable oxygen and carbon isotopes analyses. In this paper, four geochemical methods were used to analyze the properties, compositions, and isotopic ratios of the minerals in the fractures. These geochemical indicators then were used to determine the material origins and environments of the vein-forming fluids in the K_{1bs} reservoirs in the Kuqa Depression.

The CL images were obtained using a CAMBRIDGE CL8200 MK5 detector on the Zeiss microscope at the China University of Petroleum (East China). An acceleration voltage of 10 kV, 250 μA electric current, and automatic exposure time (average value from 10s to 20s) were selected to capture CL images. Optical CL has long been used to determine the brittle structure in both unmetamorphosed and metamorphosed rocks (e.g., Sprunt and Nur, 1979; Travé et al., 1998; Steven et al., 2003; Blyth et al., 2004; Holland and Urai, 2010; Lavenu et al., 2013), study diagenesis in carbonate rocks (Richter et al., 2003) and delineate fractures (e.g., Montanez, 1994; Marquez and Mountjoy, 1996; Gale et al., 2010). In addition, CL colors can qualitatively reflect subtle differences in trace- and rare earth elements concentrations and mineral textures (Pagel et al., 2000). However, quantitative analysis of minor elements and their spatial distribution require the use of higher precision instruments such as EMPA and LA-ICP-MS.

EPMA analysis was conducted using a JEOLJXA-8230 microanalyzer

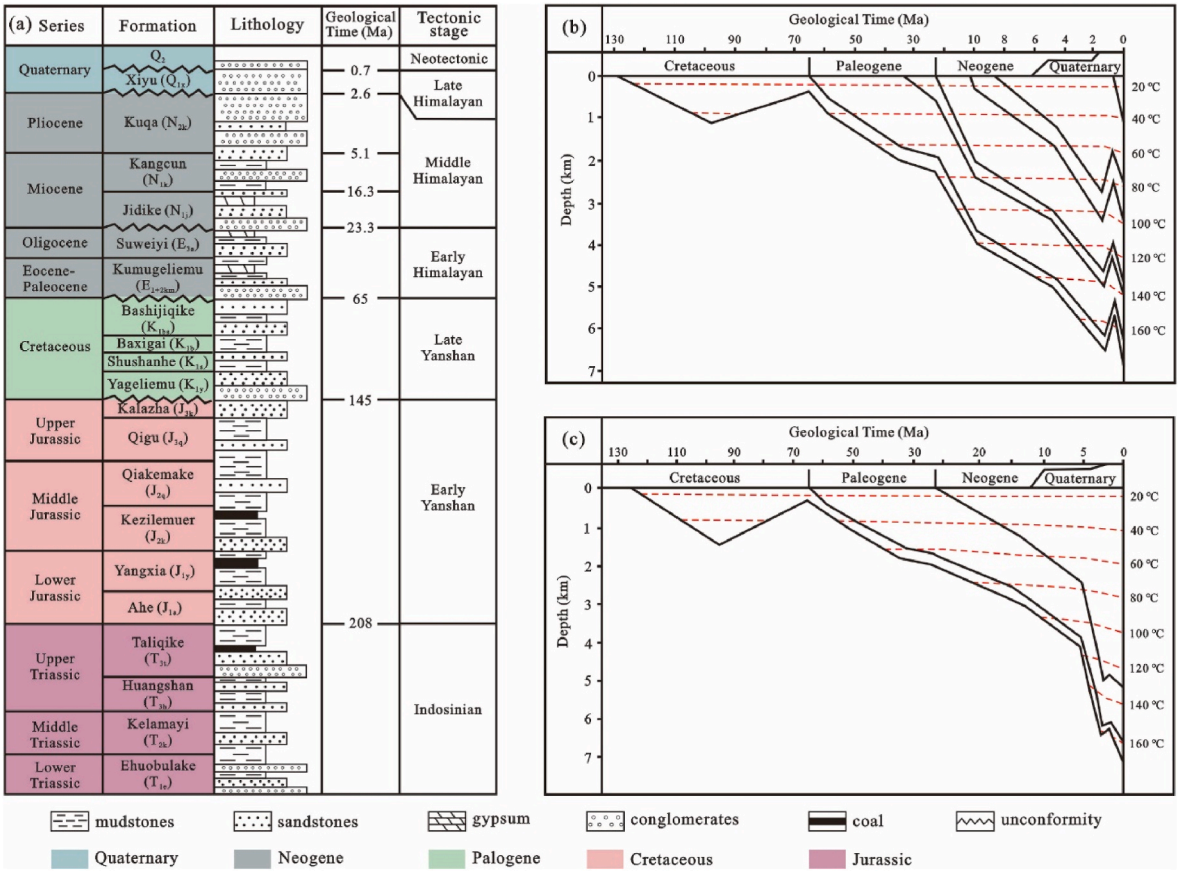

Fig. 3. (a) Simplified tectonic-stratigraphic chart of the Kuqa Depression showing key stratigraphic horizons, lithology and absolute ages (after Zeng et al., 2010; Shi et al., 2020); (b–c) Burial history curves from the Keshen and Dabei zones (after Yuan et al., 2015; Zhang et al., 2020).

at Ocean University of China using a beam spot of 10 μm diameter under 15 kV acceleration voltage and 10^{-8} A electric current. EPMA is sensitive down to ~3 wt% concentration of minor elements and ~1 wt% concentration of major elements. For carbonate minerals, EMPA can provide precise quantitative elemental concentrations of CaO and MgO. For minor elements like FeO and MnO, EMPA can provide only semi-quantitative measurement. REE and Yttrium (Y) are below the detection limit of EPMA and are measured using LA- ICP-MS.

LA-ICP-MS has been widely applied for *in situ* microanalysis of trace element contents and U–Pb dating of geological samples (Jackson et al., 1992; Fryer et al., 1993) since Gray (1984) pioneered the elemental analysis and Pb isotope dating of granites. The LA-ICP-MS analyses were done using the system in the Guiyang Laboratory of Chinese Academy of Sciences, which has a GeoLasPro laser ablation system and a detection limit (>1 ppm). The CaO concentration or percentage from EPMA as the primary parameter is used as an internal standard to correct the minor elements of calcite cements. The data processing and associated software are detailed in Liu et al. (2008) and Chen et al. (2011).

Carbon and oxygen isotopes are widely used to compare fluid sources and fluid-rock interactions (Hodson et al., 2016) due to their sensitivity to fluid compositions, mineral formation temperature, and diagenetic processes (Friedman and O'Neil, 1977; Hodson et al., 2016). Carbon and oxygen stable isotope analyses were carried out at China University of Geosciences (Wuhan). The Peedee Belemnite (PDB) standard is the references for computing carbon and oxygen isotopic ratios. The precisions of both carbon and oxygen isotope ratios are approximately ±0.2‰.

4. Results

4.1. Crystal morphology characteristics of syntaxial veins

Syntaxial mineral veins were developed in the study area. According to crystal shapes, syntaxial veins generally contain two types: blocky and elongate blocky. Blocky veins are characterized by anhedral equidimensional crystals (Fig. 5 a and b). The crystals of elongate blocky veins generally grow side by side until the fracture is completely sealed (Fig. 5 c and e). Compared to blocky veins, elongate blocky veins have higher length-width ratios and crystal growth showed certain orientations (Fig. 5 c and e). As calcite crystals grow, some crystal growth is restricted accompanying with promoted crystals, which generally grow wider. The blocky and elongate blocky veins both incorporate wall-rock fragments or whole grains from surrounding rocks (Fig. 5 a, b and d). These fragments or grains are generally rotated and have lost their initial orientations.

Syn-kinematic cement can be simultaneously deposited during fracture opening, while post-kinematic cement fills fracture voids after fracture opening (Laubach, 1988; Evans and Fischer, 2012). Syn-kinematic cement in fracture generally possess repetitive crack-seal textures, like stretched or fibrous textures and inclusion bands (Bons et al., 2012; Ukar and Laubach, 2016). Post-kinematic cementation in fractures generally is blocky or textureless (Laubach, 2003). Most euhedral quartz cements in this study show prismatic habit (Fig. 5 f), a common morphology for quartz growing into open void space. Quartz cements generally grow more readily along a- or c-axis in continuity with their quartz substrates. Some quartz cements are ideal hexagons and located in the middle of fractures without quartz substrates (Fig. 5 f-i). Occasionally, the oblique angle between thin section orientation

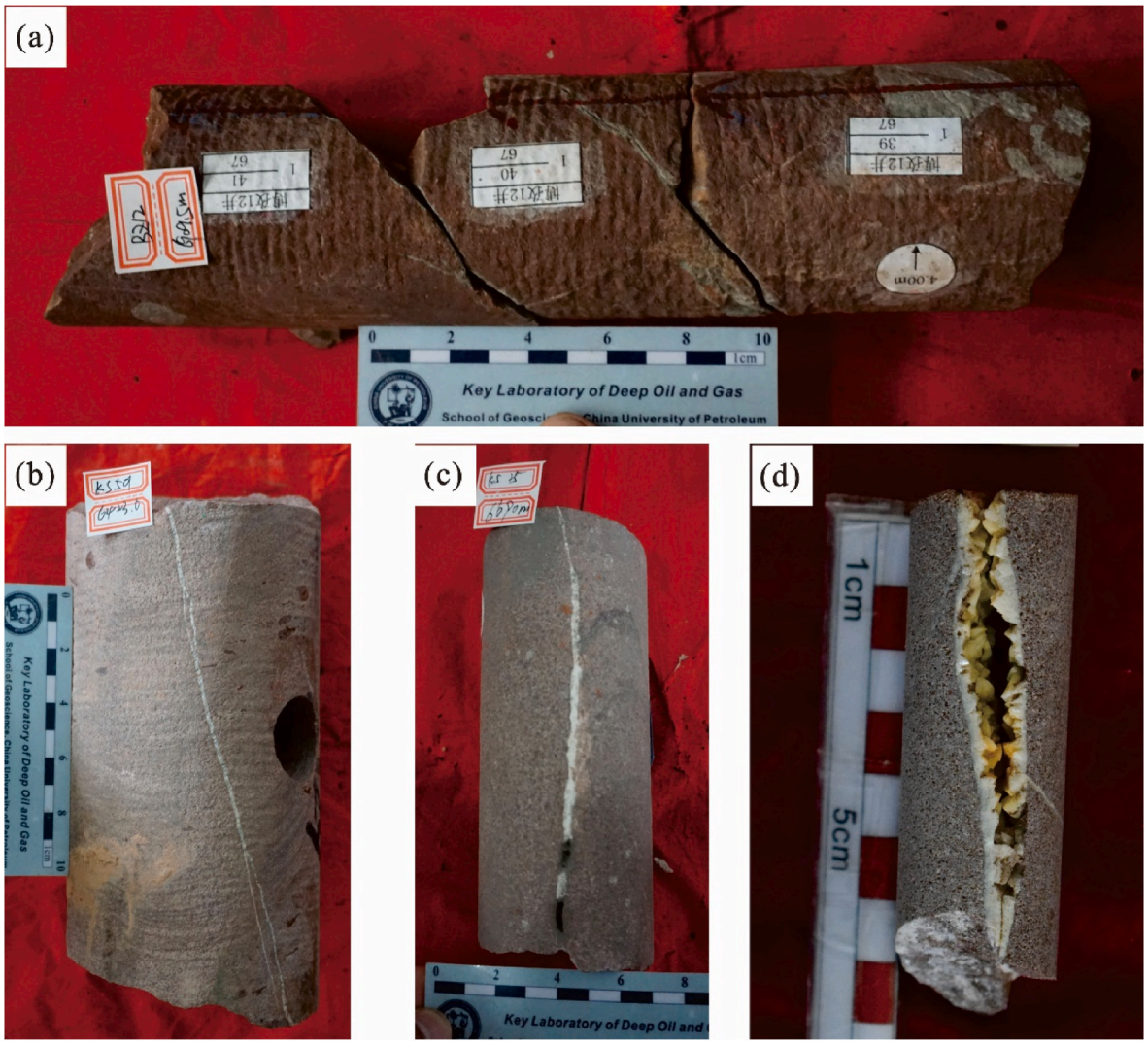

Fig. 4. (a) Open fractures from Well BZ12, 6909.5 m; (b) Completely filled tectonic fractures from Well KS501, 6423.6 m; (c–d) Partially filled fractures from Well KS25, 6690 m and Well DB304, 6878.2 m; A characteristic syntaxial vein is displayed in (d) with carbonate crystals growing from wall rock towards the center of the fracture.

and crystal growth direction may be responsible for formation of ideal hexagon quartz crystals (Lander and Laubach, 2015). In addition, an obvious inclusion band is observed between the euhedral quartz cement and substrate quartz grain (Fig. 5 g and h). Therefore, euhedral quartz cements in fractures can be regarded as syn-kinematic cements. In the fracture space, calcite cements in fractures develop straight crystal boundaries (Fig. 5 h) and possess blocky or elongate blocky shapes without obvious crack-seal textures. Most calcite veins could form by a single crack-seal event without obvious crack-seal textures and then be regarded as post-kinematic syntaxial calcite veins. In addition, one post-kinematic calcite vein possesses unique e-twinning morphology (Fig. 5 d), which appear as thin black lines under optical microscopy.

4.2. Geochemistry characteristics of calcite cements

4.2.1. Optical CL features and variations of minor elements across calcite

The calcite wall-rock cements and veins in these samples generally exhibit yellow to orange CL (Figs. 6–8). Fine variations in CL colors are primarily controlled by trace element types and concentrations (Mn^{2+} ion, Fe^{2+} ion and trivalent REE ions (esp. Sm^{3+}, Dy^{3+} and Tb^{3+}) (Richter et al., 2003; Maskenskaya et al., 2014). Consequently, *in situ* analysis of minor elements and REE + Y for two typical calcite veins and corresponding calcite wall-rock cements were performed (Figs. 6 and 7). Observations show that CL colors and intensities of both blocky veins and elongate blocky veins gradually become duller from vein margins toward vein centers. CL colors and intensity of calcite wall-rock cements generally are brighter yellow than veins.

EPMA and LA-ICP-MS are combined to quantitatively acquire minor- and rare earth element concentrations on the same individual points. Minor elements, such as Mg, Mn and Fe, are obtained by both EPMA (blue points from Figs. 6 and 7) and LA-ICP-MS (red points from Figs. 6 and 7). Low-concentration minor and rare earth elements can only be analyzed by LA-ICP-MS (red points from Figs. 6 and 7). Minor element concentrations analyzed by both EPMA and LA-ICP-MS show similar variation tendencies (Fig. 6 c-e and 7 c-e). Elemental abundances measured from LA-ICP-MS are generally higher than those obtained from EPMA. Calcite veins generally contain higher minor element concentrations, such as Mg, Mn, Fe and Sr, than calcite wall-rock cements (Fig. 6 c-f and 7 c-f). In addition, the minor element concentrations within veins decrease gradually from vein centers towards vein margins, which is similar to the trends of CL colors (Fig. 6 c-f and 7 c-f). The $\sum$REE concentrations are mostly below 600 ppm, except for some outliers, showing no distinct variations between calcite cements in fractures and wall rocks (Fig. 6 g and 7 g). The minor element distribution

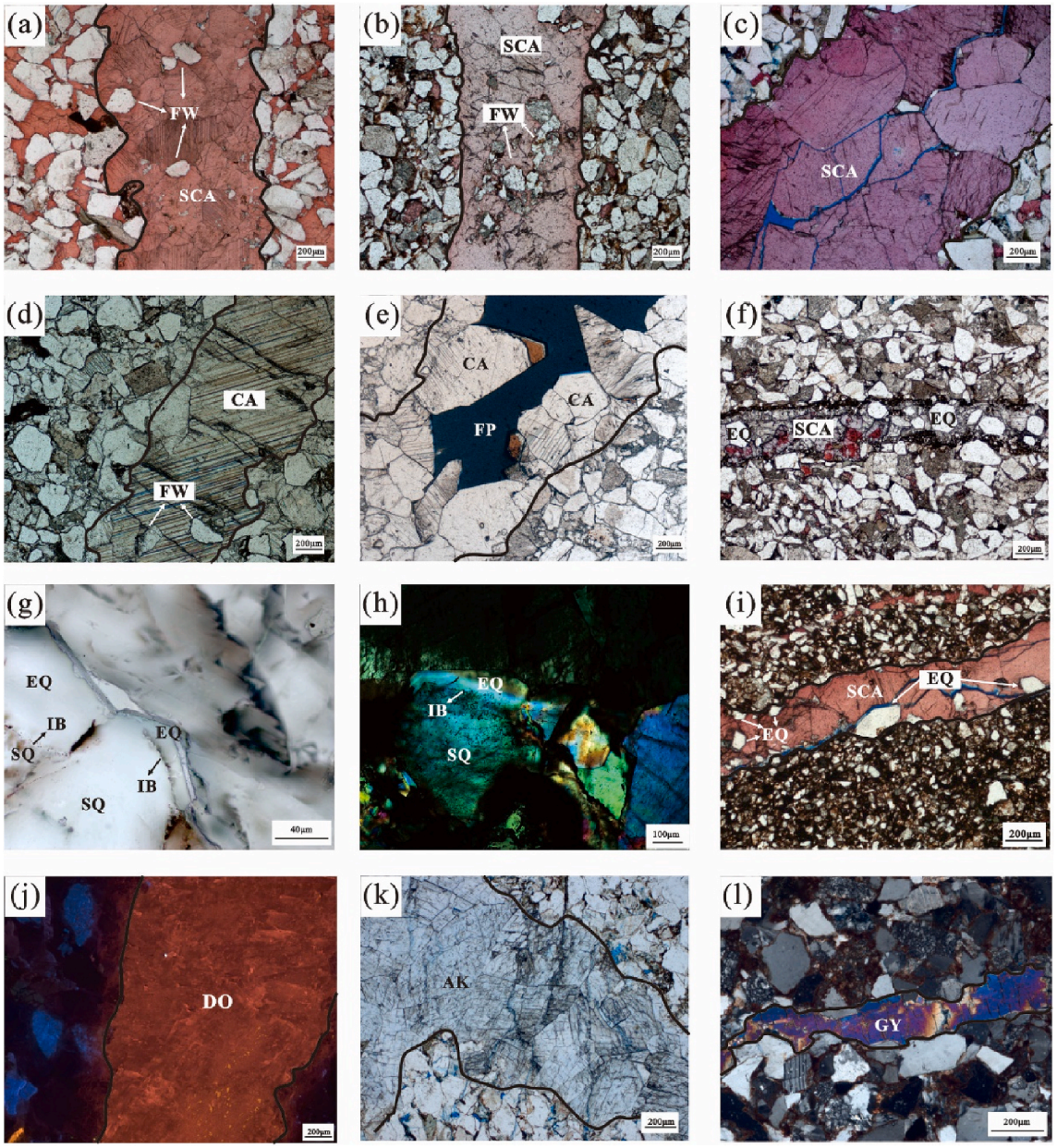

Fig. 5. (a–b) Blocky calcite vein from Well DB7, 4851.7 m, Well KS501, 6506.1 m; (c) elongate blocky to blocky calcite vein from Well DB12, 5448.9 m; (d) blocky calcite vein from Well DB9, 4851.7 m; (e) Partially filled syntaxial veins from Well DB17, 6154.2 m; (f) Integral euhedral quartz crystals within a calcite vein, Well DB12, 5448.9 m; (g–i) Euhedral quartz crystals on quartz substrates of fracture walls, Well DB304, 7030.4 m, Well DB304, 6918.6 m, Well KS10, 6232.5 m; (j) Completely filled dolomite vein, Well KS10, 6231.6 m; (k) Completely ankerite filled vein, Well DB304, 7027.6 m; (l) Completely gypsum filled vein, Well KS904, 7734.5 m. SQ-substrate of quartz grain; EQ-euhedral quartz; IB-inclusion band; SCA-stained calcite; CA-unstained calcite; DO-dolomite; GY-gypsum; AK-ankerite; FW-fragments of wall rocks; FP-fracture pores; black lines mark boundaries between veins and wall rocks. All thin sections made from core samples were provided by the Research Institute of Exploration and Development, Tarim Oilfield Company, PetroChina.

patterns of the blocky (Fig. 6) and the elongate blocky (Fig. 7) calcite veins are both characterized by convex shapes.

4.2.2. *Patterns and anomalies indicators of REE + Y*

The rare earth elements and yttrium (REE + Y) for calcite wall-rock cements and veins, including a series of lanthanoid elements (La–Lu) plus yttrium (Y), were analyzed. Because REE + Y exhibit the lanthanide contraction (Johannesson et al., 1999, 2006), the ionic radius gradually decreases as the 4f electron shell is filled. The lanthanide contraction can produce a slight fractionation among REE + Y, resulting in systemic changes of their chemical properties (Sholkovitz et al., 1989). Patterns and anomalies of REE + Y are two common indicators to describe REE + Y characteristics. However, the raw REE + Y data need to be normalized against a common reference before they can be interpreted. In this study, the Post Archean Average Shale (PAAS; McLennan, 2001) is used as the normalization reference for both types of calcite cements (e.g., Van Kranendonk et al., 2003; Kamber et al., 2004; Hohl et al., 2015).

δLa, δCe, δEu, δGd, and Y/Ho represent anomalous degrees of common rare earth elements illustrating variations of the calcite-deposition environments. δLa, δCe, δEu and δGd are calculated by Equations (1)–(4), respectively, by the geometric average method (Lawrence et al., 2006). In these equations, N represents the PAAS-normalized value, * represents this data from PAAS value.

$$\delta La = La_N/La_N^* = La_N/(Pr_N^*(Pr_N/Nd_N)^2) \quad (1)$$

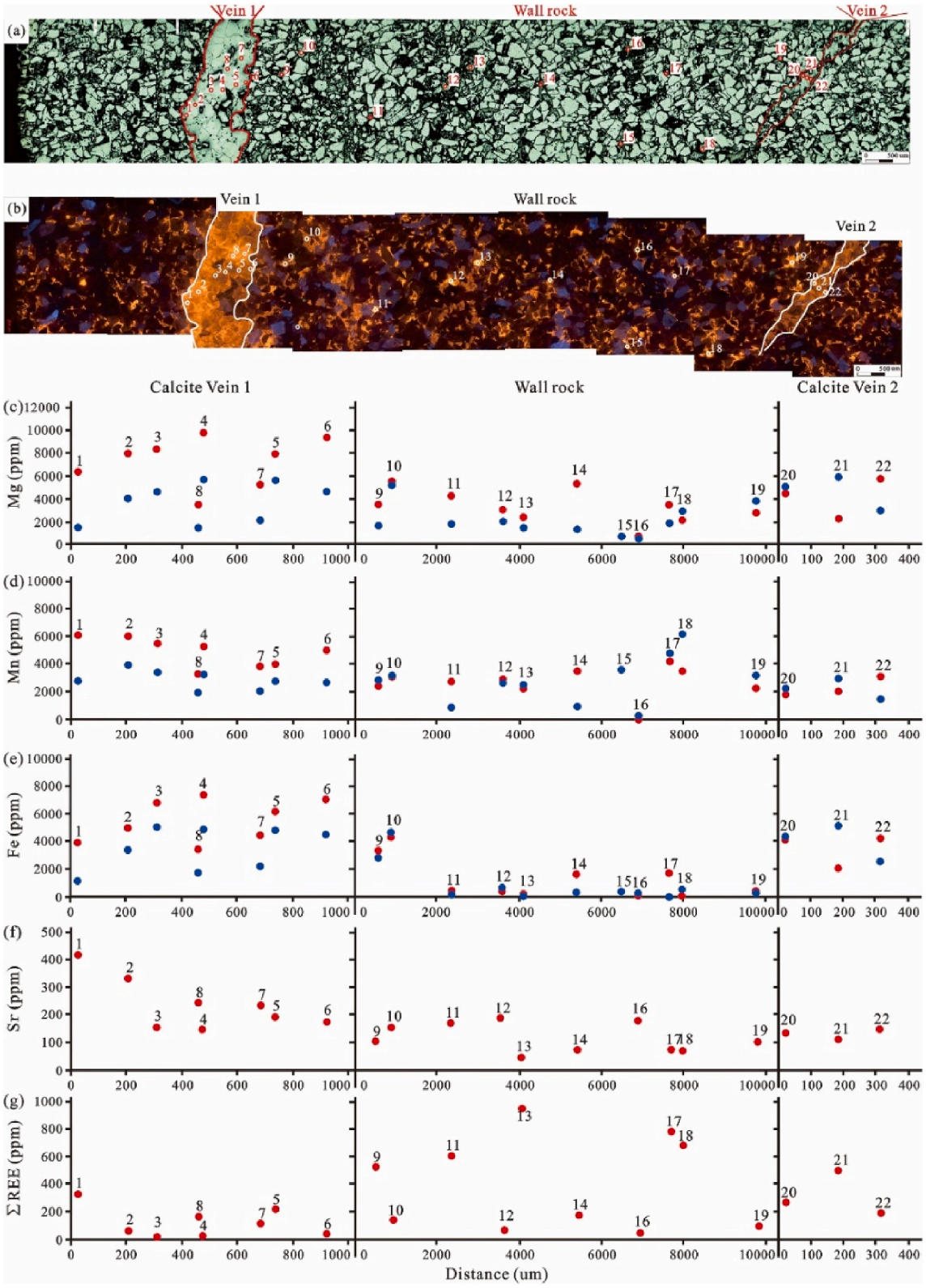

Fig. 6. Variations in the minor element distributions and concentrations in the blocky calcite vein from the DB9 well, 4851.7 m; (a–b) Images from reflected light and optical CL, respectively; (c–g) Minor element concentration variations (Mg^{2+}, Mn^{2+}, Fe^{2+}, Sr^{2+} and ∑REE) in a transect across the calcite. Blue spots denote data from EPMA, while red spots denote data from LA-ICP-MS. (For interpretation of the references to color in this figure legend, the reader is referred to the Web version of this article.)

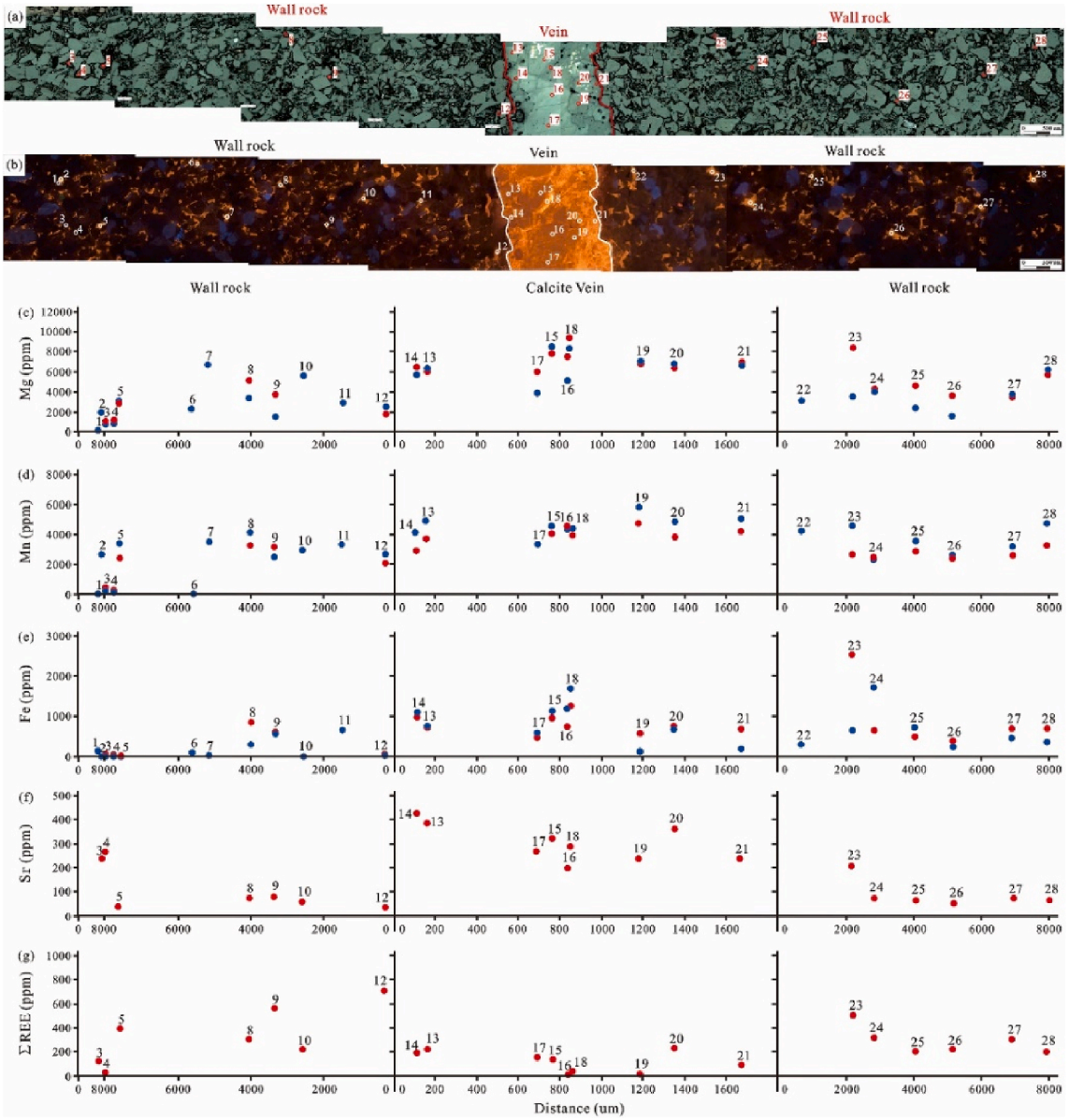

Fig. 7. Variations of minor element distributions and concentrations in the elongate blocky calcite vein from Well KS25, 6690 m; (a–b) Images from reflected light and optical CL, respectively; (c–g) Minor element concentration variations (Mg^{2+}, Mn^{2+}, Fe^{2+}, Sr^{2+} and ∑REE) in a transect across the calcite. Blue spots represent data from EPMA, while red spots represent data from LA-ICP-MS. (For interpretation of the references to color in this figure legend, the reader is referred to the Web version of this article.)

$$\delta Ce = Ce_N/Ce_N^* = Ce_N/(Pr_N^*(Pr_N/Nd_N)) \quad (2)$$

$$\delta Eu = Eu_N/Eu_N^* = Eu_N/(Sm_N^2 * Tb_N)^{1/3} \quad (3)$$

$$\delta Gd = Gd_N/Gd_N^* = Gd_N/(Tb_N^2 * Sm_N)^{1/3} \quad (4)$$

The REE + Y patterns of both the blocky calcite (Fig. 9 a) and the elongate blocky calcite veins (Fig. 10 a) show similar MREE-bulge distributions. LREE (La–Nd) and HREE (Er–Lu) are slightly depleted while MREE (Sm–Ho) is slightly enriched relative to PAAS. Only a few points in the calcite wall-rock cements (point 16 in Fig. 9 a, points 3 and 4 in Fig. 10 a) show apparent Ce depletion, while the other calcite wall-rock cements display distribution patterns and a MREE-bulge distribution similar to those of the calcite veins. Almost all δLa values for samples from calcite wall-rock cements and veins range from slightly negative to slight positive anomalies (Fig. 9 b and 10 b). Almost all calcite cements have moderately to slightly negative δCe (Fig. 9 b and 10 b) except for two calcite wall-rock cements that show slightly positive anomalies (Fig. 9 b). All calcite samples have moderately positive δEu and slightly positive δGd (Fig. 9 c and 10 c). There is no apparent correlation between δCe and δEu (Fig. 9 d and 10 d). The ratios of Y/Ho from two calcite veins mainly range from 28 to 44 and the ratios of Er/Nd show dispersive variations around 0.27 (Fig. 9 e and 10 e). In addition, the ratios of Y/Ho of the calcite wall-rock cements from the nearby Dabei Zone mainly range from 28 to 44 (Fig. 9 e), while some Y/Ho ratios from the nearby Keshen Zone are between 25 and 28 (Fig. 10 e). The ratios of Er/Nd show similar dispersive variations around 0.27 as that in the calcite veins (Fig. 9 e and 10 e).

4.2.3. Carbon and oxygen isotope characteristics

$\delta^{13}C_{PDB}$ values of calcite veins range from −3.36‰ to −1.35‰ with an average of −2.53‰, while $\delta^{13}C_{PDB}$ values of calcite wall-rock cements are between −4.76‰ and −0.81‰ with an average of −2.37‰. $\delta^{18}O_{PDB}$ values of calcite veins range from −16.43‰ to −11.37‰ with an average of −13.57‰, while $\delta^{18}O_{PDB}$ values of calcite wall-rock cements are between −14.95‰ and −9.86‰ with an average of −12.37‰.

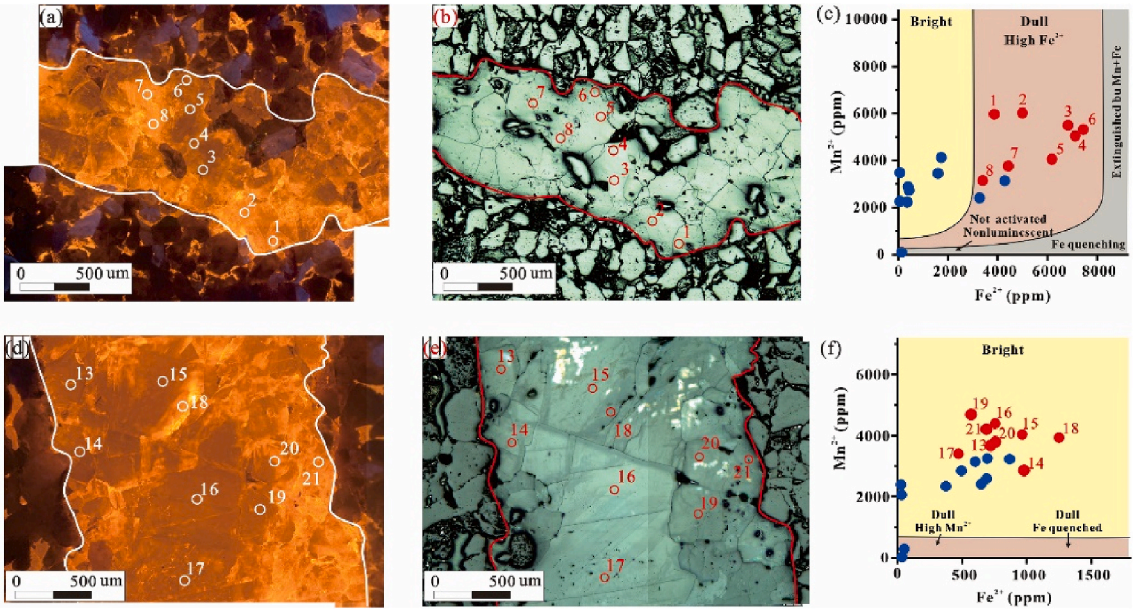

Fig. 8. (a–b) and (d–e) are enlarged images of the calcite from Fig. 6(a and b) and Fig. 7(a and b), respectively. (c) and (f) are scatter plots showing differences in Mn^{2+} and Fe^{2+} concentrations; Blue circles represent LA-ICP-MS data from calcite cement, while red circles represent LA-ICP-MS data from calcite veins. The boundaries between CL color zones are modified from Boggs and Krinsley (2006). (For interpretation of the references to color in this figure legend, the reader is referred to the Web version of this article.)

The distribution of $\delta^{13}C_{PDB}$ values in the calcite cements is more concentrated than that of $\delta^{18}O_{PDB}$ values (Fig. 11 a) and the $\delta^{18}O_{PDB}$ range of calcite wall-rock cements is more scattered than that of calcite veins. According to stable isotopes and previously reported Th results (Yuan et al., 2015; Zhang et al., 2020), two formation stages of calcite veins may be distinguished (Table 1 and Fig. 11 a). If the $\delta^{13}C_{PDB}$ and $\delta^{18}O_{PDB}$ results came from different geochemical fluids, they could show obvious differences. This means that a single outlier may represent a stage of fracture opening. While using a single point to identify a fracture opening stage may induce uncertainties, reliability of the C and O isotope results is considered high. Consequently, this outlier may be indicative of a stage of fracture opening. The paleosalinity index (Z values) of pore water can then be calculated by $\delta^{13}C_{PDB}$ and $\delta^{18}O_{PDB}$ (Equation (5); Keith and Weber, 1964) to differentiate carbonate deposited in a marine or freshwater setting (Table 1).

$$Z = a(\delta^{13}C_{PDB}+50) + b(\delta^{18}O_{PDB}+50) \quad (5)$$

Where *a* and *b* are constants of 2.048 and 0.498, respectively. The Z values can be used to semi-quantitatively reflect paleosalinity of calcite samples (Keith and Weber, 1964; Xi et al., 2019).

In order to eliminate temperature effect for oxygen isotope, reported fluid inclusion Th ranges of calcite veins (Yuan et al., 2015; Zhang et al., 2020) are used to calculate the $\delta^{18}O_{SMOW}$ of vein-forming fluid (Fig. 11 b and Table 1) and further infer fluid origins (Fig. 11 c) according to the calcite fractionation equation (Dietzel et al., 2009). The $\delta^{18}O_{PDB}$ values of the vein-forming fluids can then be calculated from these calculated $\delta^{18}O_{SMOW}$ values using the empirical equation: $\delta^{18}O_{SMOW} = 1.03086*\delta^{18}O_{PDB}+30.86$, recommended by the United States Geological Survey. The $\delta^{18}O_{PDB}$ and $\delta^{13}C_{PDB}$ can be used to calculate the Z values and semi-quantitatively evaluate paleosalinity of pore water. Z values of calcite veins range from 102.52 to 111.54 (Table 1). Due to the lack of fluid inclusion Th values from the calcite wall-rock cements, $\delta^{18}O_{SMOW}$ and Z values of calcite wall-rock cements cannot be acquired.

5. Discussion

Tectonic veins may form concurrently with or slightly lagging fracture opening, or they may be deposited long after fractures ceased opening (Laubach, 2003). Evidence in the form of textures within veins, or overlapping relationships among mineral phases, are needed to determine when deposits formed relative to fracture opening (Fig. 1). The presence of some textures such as "stretched crystals" or "crack-seal texture" depend on crystal growth rates compared to fracture opening rates (i.e., spanning potential, Lander and Laubach, 2015). Consequently, some mineral deposits that accumulate in opening fractures may lack textural evidence that the deposits formed during fracture opening (Fig. 1b).

For deposits formed contemporaneously with opening, geochemical compositions can be linked to the formation fluids present during opening. Fine-scale geochemical investigation may provide important clues on the origin, types, temperature-pressure regimes and evolution of deposit-forming fluids (e.g., Jensenius and Burruss, 1990; Lee and Morse, 1999; Budai et al., 2002; Blyth et al., 2004, 2009; Holland and Urai, 2010; Cobbold et al., 2013; Fall et al., 2015) and thus conditions existing when fractures were active. Elemental fluctuations or concentrations may indicate potential fluid origin, for example, meteoric water usually contains higher Mn, Fe and lower Sr than that of seawater (Liu et al., 2010; Shen et al., 2010). The concentration of transition metals (e.g., Fe, Mn, Zn, Pb etc.) tends to increase with enhanced fluid-rock interactions at elevated temperature and chlorinity (Yardley, 2013). These interactions may also be influenced by elemental partition coefficients within different fluids and carbonate minerals, and element concentrations in the solution (Brand and Veizer, 1980). In addition, rare earth element indicators from REE + Y patterns and common anomalies may be used to infer fluid types (e.g., seawater, meteoric water or hydrothermal fluids), pH and redox environments (Lawrence et al., 2006; Debruyne et al., 2016). Stable carbon and oxygen isotopes are known to be effective tools in identifying fluid origin, types of precipitation environment and fluid-rock interaction degrees (Bons et al., 2012; Maskenskaya et al., 2014; Xi et al., 2019). Primary fluid inclusion homogenization temperatures (Th) without late diagenetic alteration are commonly employed to derive $\delta^{18}O_{SMOW}$ values of the parent fluids (Goldstein, 2001, p. 201; Mangenot et al., 2017). Potential fluid origin can thus be inferred by using the $\delta^{13}C_{PDB}$ and $\delta^{18}O_{SMOW}$ values.

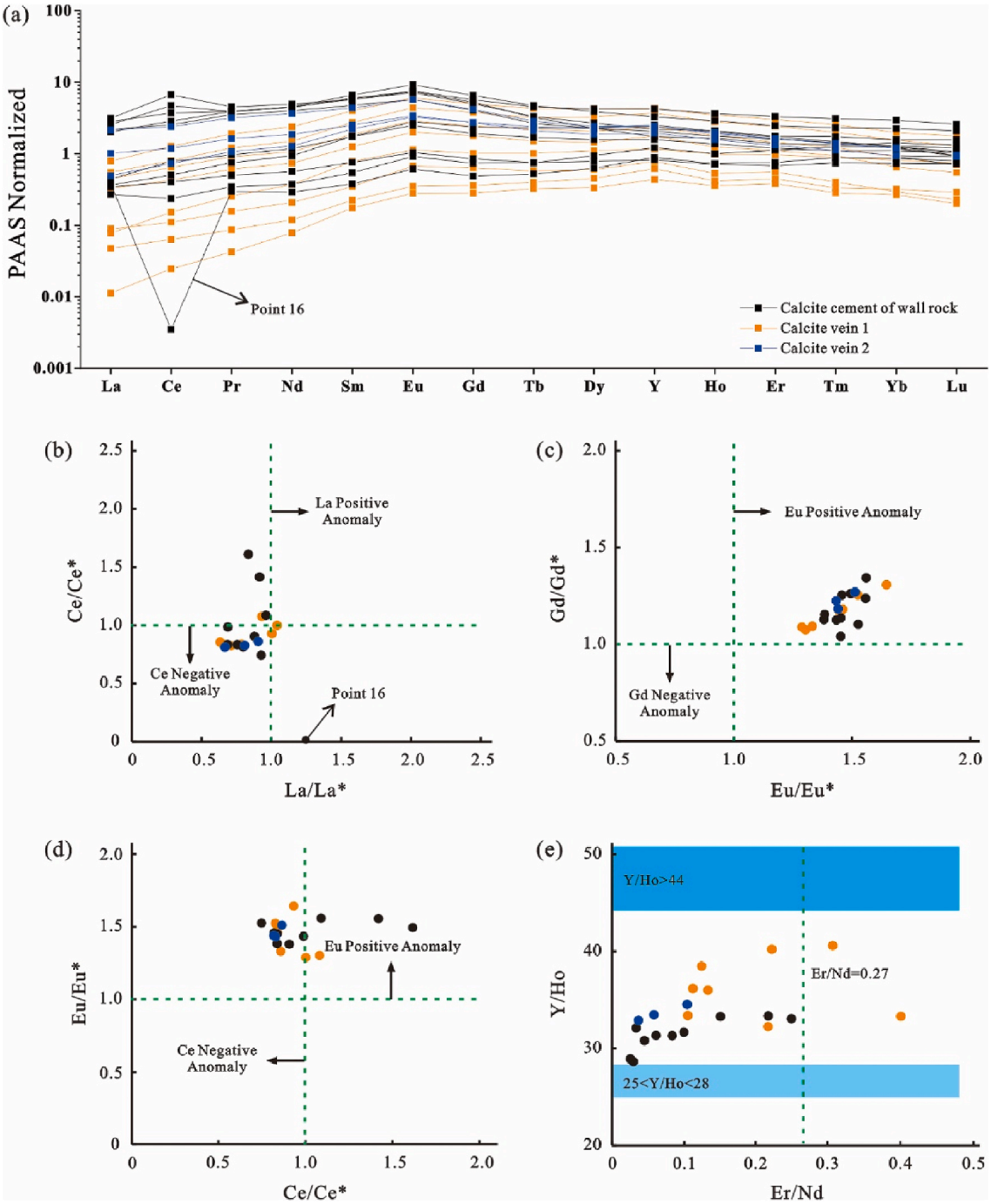

Fig. 9. REE + Y pattern of PAAS-normalized data and common anomalies of blocky calcite in fractures and adjacent calcite cements in wall rocks (Well DB9, 4851.7 m). (a) Wall-rock cements and veins mainly display MREE-bulge patterns after PAAS normalization; (b–e) Distribution characteristics of common anomalies (δREE >1 indicates positive anomaly, while δREE <1 represents negative anomaly).

5.1. Implications from the microstructures of syntaxial veins

Syntaxial veins are usually considered to form in the void space formed by extensional strain. Under a regional compressional stress, they mainly appear at the crests of thrust anticlines (Figs. 1 and 4), where local extensional stress is present. Meanwhile, fluid overpressure caused by shortening horizons can also promote fracture opening and mineral deposition (Eckert et al., 2014). Crystals in syntaxial veins generally grow symmetrically from wall rocks into the open fracture space, but occasionally crystals can grow from one side of wall rock towards the other. As veins are sealed, the difference between fracture opening rates and crystal growth rates can result in differences in the extent of sealing (i.e., open, partially filled or completely filled).

Although blocky and elongate blocky veins can both form under similar mechanical conditions, they show different crystal shapes. Continuous crystal nucleation with/without substrates in an oversaturated fluid can lead to the development of a blocky crystal shape. Different growth rates of calcite crystals that lack space to grow due to their crystal habits could form unequal granular blocky crystals. When crystal growth rates are slower than the fracture opening rates, some crystals gradually become narrower while others can form elongate-blocky or blade-like crystals along the growth direction of crystals.

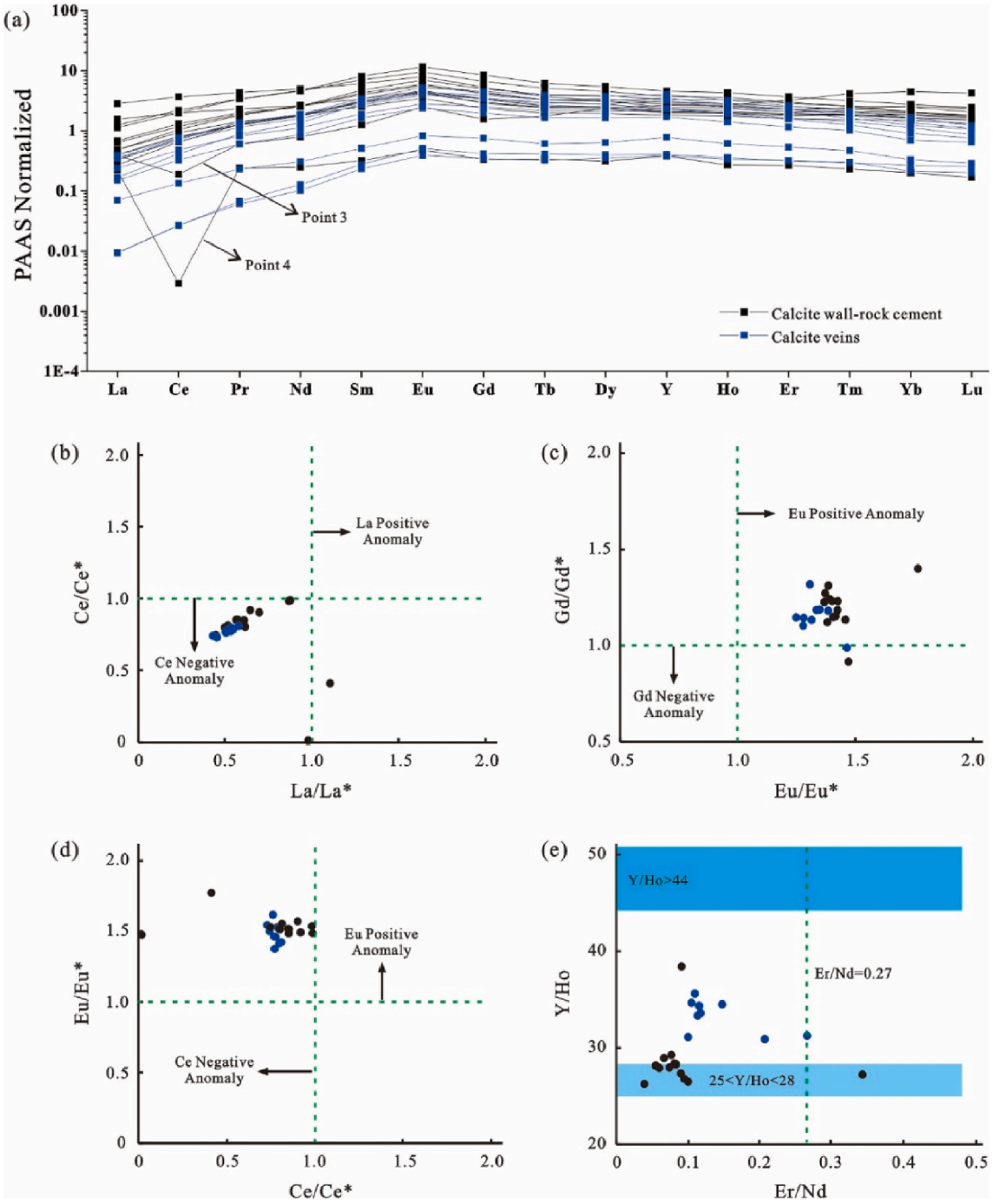

Fig. 10. REE + Y pattern of PAAS-normalized data and common anomalies of blocky calcite veins in fractures and adjacent calcite cements in wall rocks (Well KS25, 6690 m). (a) Wall-rock cements and veins mainly show MREE-bulge patterns after PAAS normalization; (b–e) Distribution characteristics of common anomalies (δREE >1 indicates positive anomaly, while δREE <1 represents negative anomaly).

This phenomenon results in a crystallographic preferred orientation (CPO) (Bons et al., 2012). The crystal growth competition present in elongate blocky veins may imply that crystals grow into a fluid-filled crack.

5.2. Variations of CL colors and trace-element concentrations within syntaxial veins

For carbonate cement, long CL wavelengths ranging from yellow to red light require longer time to decay after excitation by the electron beam (Boggs and Krinsley, 2006; Ukar and Laubach, 2016). This phenomenon is termed phosphorescence (Reed and Milliken, 2003; Lee et al., 2005), which is a key factor activating yellow to red CL of calcites. Therefore, optical CL can be conveniently used to map carbonate cement in fractures (e.g., Travé et al., 1998; Rimsa et al., 2007; Holland and Urai, 2010; Lavenu et al., 2013). Emissions of CL are primarily controlled by trace element types and concentrations. The variations in the CL intensity can thus reflect the chemical characteristics of carbonate-forming fluids and their evolution during the carbonate cement precipitation. Mn^{2+} ion and trivalent REE ions (esp. Sm^{3+}, Dy^{3+} and Tb^{3+}) appear to be the most important activators for extrinsic CL, whereas Fe^{2+} is the principal quencher (Richter et al., 2003;

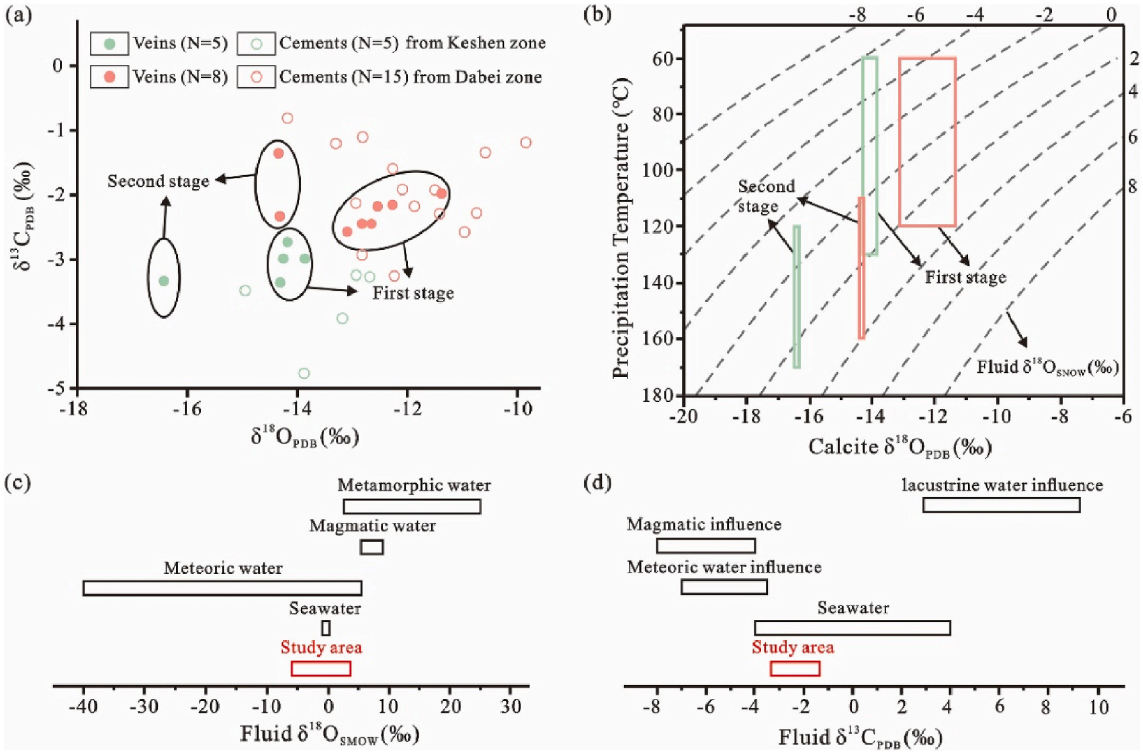

Fig. 11. (a) Carbon and oxygen isotopes of calcite cements in wall rocks and fractures; (b) Oxygen isotopic fractionation curve with increasing precipitation temperature (from Friedman and O'Neil, 1977); (c) Ranges of fluid $\delta^{18}O_{SMOW}$ value for potential oxygen sources (after Rollinson, 1993 and references therein); (d) Ranges of $\delta^{13}C_{PDB}$ value for potential carbon sources (after Xi et al., 2019 and references therein).

Table 1
Carbon and oxygen isotope compositions, $\delta^{18}O_{SMOW}$ range of the parent fluid and Z value range of calcite veins. The minimum and maximum values for the oxygen isotope ratios of the parent fluids are a function of the range of Th values. Homogenization temperature range modified from Yuan et al. (2015); Zhang et al. (2020).

Zone	Vein formation stage	Well	Depth, m	$\delta^{13}C_{PDB}$ ‰	$\delta^{18}O_{PDB}$ ‰	Th value ranges °C	$\delta^{18}O_{SMOW}$ of parent fluid ‰		$\delta^{18}O_{PDB}$ of parent fluid ‰		Z values	
							minimum	maximum	minimum	maximum	minimum	maximum
Dabei	First	DB12	5397	−2.448	−12.825	60–120	−4.66	2.39	−34.50	−27.66	105.10	108.51
		DB12	5401	−2.447	−12.654		−4.49	2.57	−34.33	−27.49	105.19	108.60
		DB12	5401.8	−2.157	−12.272		−4.10	2.95	−33.96	−27.11	105.97	109.38
		DB9	4846.1	−2.179	−12.545		−4.38	2.68	−34.23	−27.38	105.79	109.20
		DB9	4851.7	−2.572	−13.096		−4.93	2.12	−34.77	−27.93	104.72	108.13
		DB17	6154.2	−1.977	−11.374		−3.20	3.87	−33.08	−26.23	106.78	110.19
	Second	DB12	5442.3	−2.329	−14.317	110–160	−0.07	4.05	−30.05	−26.05	107.56	109.56
		DB304	7077.5	−1.354	−14.341		−0.10	4.03	−30.08	−26.07	109.55	111.54
Keshen	First	KS10	6312.3	−2.993	−14.257	60–130	−6.10	1.82	−35.90	−28.21	103.29	107.12
		KS10	6379.6	−2.731	−14.180		−6.03	1.90	−35.83	−28.14	103.87	107.69
		KS25	6688	−2.991	−13.865		−5.71	2.22	−35.52	−27.83	103.49	107.32
		KS25	6690	−3.358	−14.312		−6.16	1.76	−35.96	−28.27	102.52	106.35
	Second	KS501	6505.2	−3.336	−16.431	120–170	−1.27	2.56	−31.21	−27.49	104.92	106.78

Maskenskaya et al., 2014).

The intensity of REE-activated luminescence is generally much lower in sedimentary calcite than that of hydrothermal calcite because sedimentary calcites contain insufficient REEs to activate CL (Figs. 6 and 7). Since the emission spectra of REEs and Mn^{2+} overlap extensively, CL activated by low-concentrations of REEs can be obscured by high concentration of Mn^{2+} (Habermann et al., 1996). Consequently, the CL colors and intensities can be controlled in large part by the potential relationship between Mn^{2+} and Fe^{2+} concentrations in K_{1bs} in the Kuqa Depression. A cross-plot of CL intensity versus Mn^{2+} and Fe^{2+} concentrations in calcite and dolomite (Fig. 8) has previously been established on the basis of empirical data (Machel et al., 1991; Machel, 2000). Therefore, the intensity of CL emissions is a complex function of moderate Mn^{2+} concentration activation, quenched by $Fe^{2+}$and high concentration of Mn^{2+} ions.

Although both blocky and elongate blocky calcite veins show bright- to dull-orange CL colors (Fig. 8 a and d), they contain variable Mn^{2+} content (3000–6000 ppm). Highly variable Fe^{2+} content (500–8000 ppm) could therefore be responsible for the dull CL. The Fe^{2+} concentrations within a calcite vein gradually increase from the outer vein to the inner vein (Fig. 6 b-c and 7 b-c). This distribution occurs since Fe^{2+} is usually precipitated at the final stage of calcite vein precipitation in the form of Fe oxide/hydroxides (Maskenskaya et al., 2014). In addition, the Mg^{2+}, Mn^{2+} and Sr^{2+} concentrations show the same distributions as Fe^{2+} within individual veins. This suggests that the ratios of concentrations among Mg^{2+}, Mn^{2+}, Sr^{2+} and Fe^{2+} are relatively constant in the vein-forming fluid during the growth of calcite crystals. As a result, the increase in the minor element concentrations from vein wall to the inner

vein could be common for the syntaxial veins, regardless of whether the vein is of blocky or elongate blocky crystal morphology. Trace-element variations can occur even over a 200 μm distance and could produce large fluctuations to influence CL colors and intensities (Samples 4, 5, 7, 8 in the blocky calcite vein; Fig. 6). Such trace-element variations within a single vein may be associated with variability in trace elements in the precipitation solution (Denniston et al., 1997; Barker et al., 2006), trace-element incorporation rates in calcite due to different crystallization conditions (Denniston et al., 1997; Barker et al., 2006), fluid flow rates (Maskenskaya et al., 2014), the mixture of exotic fluids with various chemistries induced by tectonic movement (Wogelius et al., 1997; Debruyne et al., 2016), and changes in the redox potential and clay-mineral diagenesis.

5.3. Parent fluid geochemical characteristics and material sources

Minor elements, REEs and carbon and oxygen stable isotopes have been collectively used to identify possible subsurface fluid environment evolution and the origins of the precipitating materials. The connate or initial waters, accompanying sediments at the time of deposition, are generally theoretical and conceptual, because of later complicated geochemical influences by various geological processes (Morad et al., 1999). Parent fluids are defined as the entire fluid volume from which the analyzed crystals and co-precipitating phases originated (Debruyne et al., 2016). Therefore, several geochemical tools can be applied to probe calcite cements in wall rocks and fractures to reconstruct the parent fluid compositions.

5.3.1. Interpretation of REE + Y distributions and common anomalies

The similarity and contrast of trace elements and isotope ratios between calcite wall-rock cements and calcite veins can provide insights on whether vein material originated or inherited from the surrounding wall rocks. For example, quartz particles of wall rock are likely to be a major contributor to quartz cement in fractures, but other silicates (e.g., clays, feldspars) may also contribute to quartz veins. Except for minor amounts of calcite wall-rock cements that show apparent negative δCe, most calcite wall-rock cements and veins exhibit MREE-bulge distributions (Fig. 9 a and 10 a), which are similar to features of sedimentary pore fluid (Grandjean et al., 1987; Kidder and Eddy-Dilek, 1994; Kidder et al., 2003; Bright et al., 2009). In addition, the non-correlation between δCe and δEu (Fig. 9 c and 10 c) may indicate that late diagenetic alteration had little influence on the REE + Y distributions of authigenic carbonate (Shields and Webb, 2004).

Apart from REE + Y patterns, common anomalies may also imply potential fluid origins. Both the calcite wall-rock cements and veins show similar common features: (1) moderately-slightly negative δLa anomalies (Fig. 9 b and 10 b); (2) moderately-slightly negative δCe anomalies (Fig. 9 b and 10 b); (3) moderately positive δGd anomalies (Fig. 9 c and 10 c); (4) moderately positive δLu anomalies (Fig. 9 c and 10 c); (5) no apparent correlation between δCe and δEu; (6) scattered Y/Ho ratios between 28 and 44, with values that are generally higher than that of calcite wall-rock cements (Fig. 9 d and 10 d); and (7) variably scattered Er/Nd ratios (Fig. 9 d and 10 d).

The largest inter-elemental fractionations are associated with Ce and Eu, since certain redox environments can induce changes of elemental valences (German and Elderfield, 1989; Bau and Möller, 1992; Holser, 1997). Generally, Ce^{3+} in sub-aerial environments is oxidized to Ce^{4+}. As a result, a negative δCe may indicate oxidizing fluid conditions (German and Elderfield, 1989; Holser, 1997). Most calcite wall-rock cements and veins of K_{1bs} have slightly to moderately negative δCe (Figs. 9 and 10), which is consistent with inheritance from weakly oxidizing seawater. At low mineralization temperatures, Eu is normally trivalent (Debruyne et al., 2016). Most of the samples from K_{1bs} show positive δEu (Figs. 9 and 10), implying a divalent state of Eu in calcite wall-rock cements and veins rather than a trivalent one. Preferential leaching of Eu-rich material like feldspar, reducing conditions during calcite deposition and increasingly divalent state of Eu with temperature (generally found in hydrothermal fluids, $T > 250$ °C) are important factors to influence the positive degree of δEu (Sverjensky, 1984; Bau and Möller, 1992). In addition, raw REE data after PAAS normalization may also induce slightly higher δEu compared with other normalization materials (Debruyne et al., 2016). Due to the lack of evidence of hydrothermal fluid injection and the possible weak oxidizing environment inferred from negative δCe values, preferential leaching of Eu-rich material from feldspar is the preferred interpretation for the moderately positive δEu.

Modern sea water and river water commonly show positive δLa and δGd (Elderfield et al., 1990; Bau and Dulski, 1996; Lawrence et al., 2006; Zhao et al., 2019). δLa values are also dependent on the solution pH value and δLa becomes negative when $pH < 6.5$ (Lawrence et al., 2006; Zhao et al., 2019). These samples mostly show negative δLa anomalies, implying a weak-acidic solution origin like meteoric water. Sea water and river water with positive δLa anomalies may be partially incorporated. The moderately positive δGd anomalies are incorporated into calcite veins and wall-rock cements. Previous studies demonstrated positive δGd anomalies may be of anthropogenic origin (Bau and Dulski, 1996; Nozaki et al., 2000) and be induced after PAAS normalization (De Baar et al., 1985). However, since these samples are from drilling cores, an anthropogenic influence on δGd can be excluded.

Y/Ho and Er/Hd ratios are generally used to determine potential fluid origins from river water or sea water (Fig. 9 e and 10 e) (De Baar et al., 1985; Nozaki et al., 1997; Bolhar and Van Kranendonk, 2007). Y/Ho ratios of calcite wall-rock cements show variable distributions ranging from 26 to 39, consistent with a mixture of river water ($25 < Y/Ho < 28$) and sea water ($Y/Ho > 44$). Y/Ho ratios of most calcite veins investigated range from 30 to 40, indicating an increasing sea water contribution compared to calcite wall-rock cements. Er/Hd ratios can also be used as a reference to identify fluid types; normal seawater has an Er/Hd ratio of 0.27 (de Baar et al., 1988). These calcite samples including both calcite wall-rock cements and veins are characterized by variable Er/Hd (Fig. 9 e and 10 e), implying that other types of fluids may be incorporated along with seawater.

REE + Y patterns and common REE + Y anomalies may provide insights for geochemical features of the parent fluids. Overall, calcite wall-rock cements and veins show no evidence of contribution from fluids other than the original pore fluids, meteoric water and seawater. This mixed parent fluid shows an acidic and oxidizing character during the calcite deposition.

5.3.2. Interpretation of stable carbon and oxygen isotopes

The $\delta^{13}C$ and $\delta^{18}O$ values plus the fluid inclusion Th data can indicate the types and potential origins of the parent fluids. Th values are regarded as crystallization temperatures as suggested by Hrabovszki et al. (2022). However, the calculated $\delta^{18}O_{SMOW}$ values of parent fluids are generally underestimated, since the Th values without pressure correction represent the minimum trapping temperatures (Goldstein and Reynolds, 1994; Diamond, 2003). The $\delta^{13}C$ ranges of calcite wall-rock cements and veins mostly overlap (Fig. 11 a) and are similar to the $\delta^{13}C$ range of sea water (Fig. 11 d). In addition, two stages of calcite vein formation in K_{1bs} are recognized from fluid inclusions and oxygen-isotope ratios (Fig. 11 a). The $\delta^{18}O_{SMOW}$ values of possible parent fluids can be calculated by the calcite-water fractionation equation (Dietzel et al., 2009) (Fig. 11 b) and their range is consistent with $\delta^{18}O_{SMOW}$ ranges of sea water and meteoric water (Fig. 10 c). Although possible sources of parent fluids, seawater and meteoric water, can be inferred, the fluid origin is often not unique, because the $\delta^{18}O_{SMOW}$ range of various fluids may overlap each other (Fig. 11 c), and their signatures could also be masked by fluid-rock interaction and fluid mixing.

In addition, the range of stable isotope ratios can be used to discriminate whether the fluid environment is relatively closed or open. If the stable isotopes ratio range scatters within 3‰, the fluid

geochemistry and temperature may be regarded as constant (Lee et al., 1997; Barker et al., 2006) and are possibly buffered by wall rocks over geological time scales (Hilgers and Sindern, 2005; Smith et al., 2014). This would indicate a relatively closed and stable fluid environment. In contrast, if stable isotope ratios show strong fluctuations (>6‰), various degrees of fluid-rock interactions may have occurred (Rye and Bradbury, 1988) or a mixture of different fluid types was present (Wogelius et al., 1997). This may indicate a relatively open fluid environment. The $\delta^{13}C_{PDB}$ and $\delta^{18}O_{SMOW}$ ranges of calcite cements in wall rocks and fractures fluctuate within 4‰, showing no extreme variations (Fig. 11 a). This may indicate a relative stable fluid chemistry and temperature (Lee et al., 1997) buffered by the wall rocks, or a rapid crystallization of individual veins preventing effective isotopic fluid-rock exchange and/or temperature exchange (Katz et al., 2006). Consequently, if the injection of exotic fluids and short-term intensive effect of fluid-rock interactions can be excluded, the calcite veins may have been directly precipitated from the parent fluid under a relatively stable and closed geochemical condition.

The Z value was originally derived from carbonate by selecting samples which could be certainly classified into marine or freshwater (Keith and Weber, 1964). Therefore, this indicator has been often used to discriminate carbonates sourced from seawater (>120) or fresh water (<120) (Hofer et al., 2013; Veras et al., 2021). That the calcite veins were precipitated from deep pore fluids without mixing of exotic fluids was demonstrated by stable isotope variation and structural evolution. Therefore, oxygen isotope changes mainly caused by increasing temperature could be an important factor for Z values calculation. Th data, the calcite fractionation equation and empirical equation between $\delta^{18}O_{PDB}$ and $\delta^{18}O_{SMOW}$ can be used to eliminate the temperature effect and obtain $\delta^{18}O_{PDB}$ values of the parent fluid that range from −35.96‰ to −26.05‰ (Table 1). The Z values calculated from $\delta^{13}C_{PDB}$ and $\delta^{18}O_{PDB}$ can indicate the fluid paleosalinity during the formation of calcite veins. The Z values of calcite veins range from 102.52 to 111.54 (Table 1), suggesting that calcite veins in the study area have inherited properties from fresh water (Keith and Weber, 1964; Zhang et al., 2020). Considering the results of $\delta^{13}C_{PDB}$, $\delta^{18}O_{SMOW}$ and Z values together, meteoric water appears to be a dominant part of the parent fluid with a minor contribution from seawater. As the K_{1bs} Formation was gradually buried and only weakly deformed, the chemical compositions of the parent fluid became stabilized and formed a relatively closed diagenetic environment.

5.4. Possible fluid evolution processes for calcite precipitation

Combining minor elements, REE + Y patterns, REE + Y anomalies, stable carbon and oxygen isotopes and Z values, the parent fluid compositions can be determined. However, the connate water characteristics during the K_{1bs} deposition cannot be effectively inferred from these geochemical data alone. Therefore, we try to combine geochemical data and a previous paleoenvironment reconstruction (Li et al., 2013) to determine possible fluid evolution processes since the deposition of the K_{1bs} Formation.

Previous studies demonstrated that in the study area the paleoenvironment had evolved from warm and moist in the early Cretaceous, with the deposition of fresh water fluvial-lacustrine sediments in the early Cretaceous in the Kuqa Depression (Guo et al., 2002) to arid and hot in the late Cretaceous (Jiang et al., 2007; Li et al., 2013). Meteoric water should thus be a major connate water for the K_{1bs} Formation in the early Cretaceous. Initially, meteoric fluid could be devoid of dissolved ions and well equilibrated with atmospheric oxygen. By dissolving minerals in the sedimentary basin, other ions and REE + Y are incorporated into the undersaturated meteoric water. This process would be limited due to weak fluid-rock interactions under a relatively low temperature and a shallow burial depth. As the entire Kuqa Depression was uplifted to the surface during the late Cretaceous, the upper Cretaceous formations were nearly completely eroded. Under a hot-arid open near-surface environment (Jiang et al., 2007; Li et al., 2013), intensive weathering and erosion caused by meteoric water would be enhanced. Feldspars would be eroded easily with the released Eu^{2+} incorporated into pore fluids (Bau and Möller, 1992). During late Cretaceous, the Tethyan Ocean transgressed eastwards and flooded the lower remaining Cretaceous formations in the Kuqa Depression (Guo et al., 2002). High volumes of Cretaceous oxidizing surface seawater could then be mixed with pore fluids in the Cretaceous units, adding abundant Ce^{4+} to the K_{1bs} Formation pore fluid. This interpretation explains why both negative δCe anomalies and positive δEu anomalies are present in the calcite cements. The ranges of Y/Ho and Er/Hd ratio also suggest a mixture of seawater and fresh water. All Z values are less than 120 and further support the inference of major effect from meteoric water. After a major erosional event caused by entire uplift of Kuqa Depression at 65 Ma, the Cretaceous units continued to be buried without further intensive tectonic movements. As burial depths and horizon temperatures increased, pore water became reduced chemically and led to weaker negative δCe anomalies than those initially inherited from sea water. The $\delta^{13}C_{PDB}$ of the calcite crystals and $\delta^{18}O_{SMOW}$ of the inferred parent fluids both show relatively minor fluctuations of less than 4‰, indicating a relatively closed diagenetic environment during the precipitation of the calcite wall-rock cements and veins in the absence of exotic or/and hydrothermal fluids injection. According to previous studies of structural evolution and burial history curves, intense compression and thrust deformation occurred about 2–5 Ma ago (Graham et al., 1993; Lu et al., 1994; Yin et al., 1998; Chen et al., 2004; Boorder, 2012). Meanwhile, petroleum generation, including organic acids, potential deep magmatic fluids or hydrothermal brines could be injected into reservoirs along thrust faults (Chen et al., 2000, 2004; Jin et al., 2008). Organic acids could induce feldspar dissolution and change the chemistry of pore fluid after the formation of calcite veins. Therefore, organic acids, potential deep magmatic fluids or hydrothermal brines would not be involved and alter the chemical compositions of calcite veins.

6. Conclusions

1. Syntaxial growth is common in calcite veins developed in an ultra-deep (>6 km) reservoir in the Baishijiqike Formation, Kuqa Depression. Petrographic evidence indicates that each vein formed by a single crack-seal event. The calcite veins of typical blocky and elongate blocky crystals without obvious crack-seal textures are attributed to post-kinematic cements after fracture opening. The growth process of calcite from fracture wall to center is accompanied by variations in CL colors, CL intensities and minor element concentrations (especially the complex relationship between Mn^{2+} and Fe^{2+} ions).
2. The calcite wall-rock cements and veins inherited their compositions from the same parent fluid. This parent fluid initially evolved from a mixture of oxidizing seawater and meteoric water and was chemically reduced to a certain content under a relatively closed, deeply buried and high temperature environment. In addition, minor element concentrations increasing from vein walls to vein centers indicate an operational process of ion concentrations being gradually increased as the fracture space decreases.
3. Combining paleo-environmental studies, Tethyan Ocean transgression and structural evolution, the fresh water or meteoric water was initially retained as connate water in the K_{1bs} reservoirs in early Cretaceous. During the late Cretaceous, oxidizing surface seawater of Tethyan Ocean and meteoric water containing ions dissolved from the eroded upper Cretaceous formation entered the reservoir and altered the geochemistry of connate water. Subsequently, the entire Kuqa Depression was buried and the pore water began to be heated and reduced without exotic fluid injection. Calcite wall-rock cements and veins were then deposited from pore water and inherited its geochemistry.

Author statement

I would like to declare on behalf of my co-authors that the work described was original research that has not been published previously, and not under consideration for publication elsewhere, in whole or in part. All the authors have approved the manuscript that is enclosed and their contributions are listed below.

Shunyu WANG: Conceptualization, Methodology, Investigation, Software, Writing - Original Draft, Writing - Review & Editing.

Jian WANG: Investigation, Writing - Review & Editing, Methodology.

Keyu LIU: Writing - Review & Editing, Supervision, Project administration.

Yong LI: Validation, Formal analysis, Data Curation.

Zhenkun LI: Validation, Visualization, Data Curation.

Haijun YANG: Data Curation, Software.

Tao MO: Data Curation, Software.

Declaration of competing interest

The authors declare that they have no known competing financial interests or personal relationships that could have appeared to influence the work reported in this paper.

Data availability

Data will be made available on request.

Acknowledgements

This research is funded by the Major Research Project on the Tethys Geodynamic System from the National Science Foundation of China (Grant No. 92055204), the Chinese National Key R & D Project (2019YFC0605501) and the National Natural Science Foundation of China (Grant Nos. 42172146 and 41821002).

Appendix A. Supplementary data

Supplementary data to this article can be found online at https://doi.org/10.1016/j.jsg.2023.104895.

References

Barker, S., Cox, S., Eggins, S., Gagan, M., 2006. Microchemical evidence for episodic growth of antitaxial veins during fracture-controlled fluid flow. Earth Planet Sci. Lett. 250, 331–344. https://doi.org/10.1016/j.epsl.2006.07.051.

Barker, S.L.L., Bennett, V.C., Cox, S.F., Norman, M.D., Gagan, M.K., 2009. Sm–Nd, Sr, C and O isotope systematics in hydrothermal calcite–fluorite veins: implications for fluid–rock reaction and geochronology. Chem. Geol. 268, 58–66. https://doi.org/10.1016/j.chemgeo.2009.07.009.

Bau, M., Dulski, P., 1996. Distribution of yttrium and rare-earth elements in the Penge and Kuruman iron-formations, Transvaal Supergroup, South Africa. Geol. Geochem. Transvaal Supergr. 79, 37–55. https://doi.org/10.1016/0301-9268(95)00087-9.

Bau, M., Möller, P., 1992. Rare earth element fractionation in metamorphogenic hydrothermal calcite, magnesite and siderite. Mineral. Petrol. 45, 231–246. https://doi.org/10.1007/BF01163114.

Becker, S.P., Eichhubl, P., Laubach, S.E., Reed, R.M., Lander, R.H., Bodnar, R.J., 2010. A 48 m.y. history of fracture opening, temperature, and fluid pressure: Cretaceous Travis Peak Formation, East Texas basin. Geol. Soc. Am. Bull. 122, 1081–1093. https://doi.org/10.1130/B30067.1.

Blyth, A., Frape, S., Ruskeeniemi, T., Blomqvist, R., 2004. Origins, closed system formation and preservation of calcites in glaciated crystalline bedrock: evidence from the Palmottu natural analogue site, Finland. Appl. Geochem. 19, 675–686. https://doi.org/10.1016/j.apgeochem.2003.07.004.

Blyth, A.R., Frape, S.K., Tullborg, E.-L., 2009. A review and comparison of fracture mineral investigations and their application to radioactive waste disposal. Appl. Geochem. 24, 821–835. https://doi.org/10.1016/j.apgeochem.2008.12.036.

Boggs, S., Krinsley, D., 2006. Application of Cathodoluminescence Imaging to the Study of Sedimentary Rocks. Cambridge University Press, Cambridge. https://doi.org/10.1017/CBO9780511535475.

Bolhar, R., Van Kranendonk, M.J., 2007. A non-marine depositional setting for the northern Fortescue Group, Pilbara Craton, inferred from trace element geochemistry of stromatolitic carbonates. Precambrian Res. 155, 229–250. https://doi.org/10.1016/j.precamres.2007.02.002.

Bons, P.D., Elburg, M.A., Gomez-Rivas, E., 2012. A review of the formation of tectonic veins and their microstructures. J. Struct. Geol. 43, 33–62. https://doi.org/10.1016/j.jsg.2012.07.005.

Boorder, H. de, 2012. Spatial and temporal distribution of the orogenic gold deposits in the Late Palaeozoic Variscides and Southern Tianshan: how orogenic are they? Ore Geol. Rev. 46, 1–31. https://doi.org/10.1016/j.oregeorev.2012.01.002.

Brand, U., Veizer, J., 1980. Chemical diagenesis of a multicomponent carbonate system; 1, Trace elements. J. Sediment. Res. 50, 1219–1236. https://doi.org/10.1306/212F7BB7-2B24-11D7-8648000102C1865D.

Bright, C.A., Cruse, A.M., Lyons, T.W., MacLeod, K.G., Glascock, M.D., Ethington, R.L., 2009. Seawater rare-earth element patterns preserved in apatite of Pennsylvanian conodonts? Geochem. Cosmochim. Acta 73, 1609–1624. https://doi.org/10.1016/j.gca.2008.12.014.

Budai, J.M., Martini, A.M., Walter, L.M., Ku, T.C.W., 2002. Fracture-fill calcite as a record of microbial methanogenesis and fluid migration: a case study from the Devonian Antrim Shale, Michigan Basin. Geofluids 2, 163–183. https://doi.org/10.1046/j.1468-8123.2002.00036.x.

Chen, J., Lu, H., Wang, S., Shang, Y., 2005. Geometric tests and their application to fault-related folds in Kuqa. J. Asian Earth Sci. 25, 473–480. https://doi.org/10.1016/j.jseaes.2004.04.008.

Chen, J., Xu, Y., Huang, D., 2000. Geochemical characteristics and origin of natural gas in Tarim Basin, China. AAPG (Am. Assoc. Pet. Geol.) Bull. 84, 591–606. https://doi.org/10.1306/C9EBCE5F-1735-11D7-8645000102C1865D.

Chen, L., Liu, Y., Hu, Z., Gao, S., Zong, K., Chen, H., 2011. Accurate determinations of fifty-four major and trace elements in carbonate by LA–ICP-MS using normalization strategy of bulk components as 100%. Chem. Geol. 284, 283–295. https://doi.org/10.1016/j.chemgeo.2011.03.007.

Chen, S., Tang, L., Jin, Z., Jia, C., Pi, X., 2004. Thrust and fold tectonics and the role of evaporites in deformation in the western Kuqa foreland of Tarim Basin, northwest China. Mar. Petrol. Geol. 21, 1027–1042. https://doi.org/10.1016/j.marpetgeo.2004.01.008.

Cobbold, P.R., Zanella, A., Rodrigues, N., Løseth, H., 2013. Bedding-parallel fibrous veins (beef and cone-in-cone): worldwide occurrence and possible significance in terms of fluid overpressure, hydrocarbon generation and mineralization. Mar. Petrol. Geol. 43, 1–20. https://doi.org/10.1016/j.marpetgeo.2013.01.010.

De Baar, H.J.W., Bacon, M.P., Brewer, P.G., Bruland, K.W., 1985. Rare earth elements in the Pacific and Atlantic oceans. Geochem. Cosmochim. Acta 49, 1943–1959. https://doi.org/10.1016/0016-7037(85)90089-4.

de Baar, H.J.W., German, C.R., Elderfield, H., van Gaans, P., 1988. Rare earth element distributions in anoxic waters of the Cariaco Trench. Geochem. Cosmochim. Acta 52, 1203–1219. https://doi.org/10.1016/0016-7037(88)90275-X.

Debruyne, D., Hulsbosch, N., Muchez, P., 2016. Unraveling rare earth element signatures in hydrothermal carbonate minerals using a source–sink system. Ore Geol. Rev. 72, 232–252. https://doi.org/10.1016/j.oregeorev.2015.07.022.

Denniston, R.F., Shearer, C.K., Layne, G.D., Vaniman, D.T., 1997. SIMS analyses of minor and trace element distributions in fracture calcite from Yucca Mountain, Nevada, USA. Geochem. Cosmochim. Acta 61, 1803–1818. https://doi.org/10.1016/S0016-7037(97)00049-5.

Diamond, L.W., 2003. Systematics of H2O inclusions. In: Samson, I., Anderson, A., Marshall, D. (Eds.), Fluid Inclusions: Analysis and Interpretation. Mineralogical Association of Canada, Ottawa.

Dickson, J.A.D., 1966. Carbonate identification and genesis as revealed by staining. J. Sediment. Res. 36, 491–505.

Dietzel, M., Tang, J., Leis, A., Köhler, S.J., 2009. Oxygen isotopic fractionation during inorganic calcite precipitation – Effects of temperature, precipitation rate and pH. Chem. Geol. 268, 107–115. https://doi.org/10.1016/j.chemgeo.2009.07.015.

Eckert, A., Connolly, P., Liu, X., 2014. Large-scale mechanical buckle fold development and the initiation of tensile fractures. G-cubed 15, 4570–4587. https://doi.org/10.1002/2014GC005502.

Elderfield, H., Upstill Goddard, R.C., Sholkovitz, E.R., 1990. The rare earth elements in rivers, estuaries, and coastal seas and their significance to the composition of ocean waters. Geochem. Cosmochim. Acta 54, 971–991. https://doi.org/10.1016/0016-7037(90)90432-K.

Evans, M.A., Fischer, M.P., 2012. On the distribution of fluids in folds: a review of controlling factors and processes. J. Struct. Geol. 44, 2–24. https://doi.org/10.1016/j.jsg.2012.08.003.

Fall, A., Eichhubl, P., Bodnar, R.J., Laubach, S.E., Davis, J.S., 2015. Natural hydraulic fracturing of tight-gas sandstone reservoirs, Piceance Basin, Colorado. Geol. Soc. Am. Bull. 127, 61–75. https://doi.org/10.1130/B31021.1.

Finkelman, R.B., Lindholm, R.C., 1972. Calcite staining; semiquantitative determination of ferrous iron. J. Sediment. Res. 42, 239–242.

Fisher, D.M., Brantley, S.L., 1992. Models of quartz overgrowth and vein formation: deformation and episodic fluid flow in an ancient subduction zone. J. Geophys. Res. 97, 20043–20061. https://doi.org/10.1029/92JB01582.

Friedman, I., O'Neil, J.R., 1977. Compilation of Stable Isotope Fractionation Factors of Geochemical Interest. US Government Printing Office.

Fryer, B.J., Jackson, S.E., Longerich, H.P., 1993. The application of laser ablation microprobe-inductively coupled plasma-mass spectrometry (LAM-ICP-MS) to in situ (U)-Pb geochronology. Chem. Geol. 109, 1–8. https://doi.org/10.1016/0009-2541(93)90058-Q.

Gale, J.F.W., Lander, R.H., Reed, R.M., Laubach, S.E., 2010. Modeling fracture porosity evolution in dolostone. J. Struct. Geol. 32, 1201–1211. https://doi.org/10.1016/j.jsg.2009.04.018.

German, C.R., Elderfield, H., 1989. Rare earth elements in Saanich Inlet, British Columbia, a seasonally anoxic basin. Geochem. Cosmochim. Acta 53, 2561–2571. https://doi.org/10.1016/0016-7037(89)90128-2.
Goldstein, R.H., 2001. Fluid inclusions in sedimentary and diagenetic systems. Lithos 55, 159–193. https://doi.org/10.1016/S0024-4937(00)00044-X.
Goldstein, R.H., Reynolds, T.J. (Eds.), 1994. Systematics of Fluid Inclusions in Diagenetic Minerals. SEPM (Society for Sedimentary Geology). https://doi.org/10.2110/scn.94.31.
Graham, S.A., Hendrix, M.S., Wang, L.B., Carroll, A.R., 1993. Collisional successor basins of western China: impact of tectonic inheritance on sand composition. GSA Bull. 105, 323–344.
Grandjean, P., Cappetta, H., Michard, A., Albarède, F., 1987. The assessment of REE patterns and 143Nd/144Nd ratios in fish remains. Earth Planet Sci. Lett. 84, 181–196. https://doi.org/10.1016/0012-821X(87)90084-7.
Gray, C.M., 1984. An isotopic mixing model for the origin of granitic rocks in southeastern Australia. Earth Planet Sci. Lett. 70, 47–60. https://doi.org/10.1016/0012-821X(84)90208-5.
Guo, X., Ding, X., He, X., Li, H., Su, X., Peng, Y., 2002. New progress in the study of marine transgressional events and marine Strata of the Meso-Cenozoic in the Tarim Basin. Acta Geol. Sin. 76, 299–307.
Habermann, D., Neuser, R.D., Richter, D.K., 1996. REE-activated cathodoluminescence of calcite and dolomite: high-resolution spectrometric analysis of CL emission (HRS-CL). Sediment. Geol. 101, 1–7. https://doi.org/10.1016/0037-0738(95)00086-0.
Hilgers, C., Sindern, S., 2005. Textural and isotopic evidence on the fluid source and transport mechanism of antitaxial fibrous microstructures from the Alps and the Appalachians: mechanisms forming antitaxial veins. Geofluids 5, 239–250. https://doi.org/10.1111/j.1468-8123.2005.00114.x.
Hilgers, C., Urai, J.L., 2005. On the arrangement of solid inclusions in fibrous veins and the role of the crack-seal mechanism. J. Struct. Geol. 27, 481–494. https://doi.org/10.1016/j.jsg.2004.10.012.
Hodson, K.R., Crider, J.G., Huntington, K.W., 2016. Temperature and composition of carbonate cements record early structural control on cementation in a nascent deformation band fault zone: Moab Fault, Utah, USA. Tectonophysics 690, 240–252. https://doi.org/10.1016/j.tecto.2016.04.032.
Hofer, G., Wagreich, M., SpÖtl, C., 2013. Carbon, oxygen and strontium isotopes as a tool to decipher marine and non-marine environments: implications from a case study of cyclic Upper Cretaceous sediments. Geol. Soc. London Special Publ. 382 (1), 123. https://doi.org/10.1144/SP382.5.
Hohl, S.V., Becker, H., Herzlieb, S., Guo, Q., 2015. Multiproxy constraints on alteration and primary compositions of Ediacaran deep-water carbonate rocks, Yangtze Platform, South China. Geochem. Cosmochim. Acta 163, 262–278. https://doi.org/10.1016/j.gca.2015.04.037.
Holland, M., Urai, J.L., 2010. Evolution of anastomosing crack–seal vein networks in limestones: insight from an exhumed high-pressure cell, Jabal Shams, Oman Mountains. J. Struct. Geol. 32, 1279–1290. https://doi.org/10.1016/j.jsg.2009.04.011.
Holser, W.T., 1997. Evaluation of the application of rare-earth elements to paleoceanography. Palaeogeogr. Palaeoclimatol. Palaeoecol. 132, 309–323. https://doi.org/10.1016/S0031-0182(97)00069-2.
Hooker, J.N., Katz, R.F., 2015. Vein spacing in extending, layered rock: the effect of synkinematic cementation. Am. J. Sci. 315, 557–588. https://doi.org/10.2475/06.2015.03.
Hrabovszki, Ervin, Tóth, Emese, Tóth, M., Tivadar, Garaguly, Istvan, Futó, István, Máthé, Zoltán, Schubert, Félix, 2022. Geochemical and microtextural properties of veins in a potential high-level radioactive waste disposal site. J. Struct. Geol., 104490 https://doi.org/10.1016/j.jsg.2021.104490.
Jackson, S.E., Longerich, H.P., Dunning, G.R., Freyer, B.J., 1992. The application of laser-ablation microprobe; inductively coupled plasma-mass spectrometry (LAM-ICP-MS) to in situ trace-element determinations in minerals. Can. Mineral. 30, 1049–1064.
Jensenius, J., Burruss, R.C., 1990. Hydrocarbon-water interactions during brine migration: evidence from hydrocarbon inclusions in calcite cements from Danish North Sea oil fields. Geochem. Cosmochim. Acta 54, 705–713. https://doi.org/10.1016/0016-7037(90)90366-S.
Jia, D., Lu, H., Cai, D., Wu, S., Shi, Y., Chen, C., 1998. Structural features of northern Tarim Basin: implications for regional tectonics and petroleum traps. AAPG (Am. Assoc. Pet. Geol.) Bull. 82, 147–159.
Jiang, D., Wang, Y., Wei, J., 2007. Palyofloras and their environmental significance of the early Cretaceous in Wuqia, Xinjiang Autonomous regin. J. Palaeogeogr. 9, 185–196.
Jin, Z., Yang, M., Lu, X., Sun, D., Tang, X., Peng, G., Lei, G., 2008. The tectonics and petroleum system of the Qiulitagh fold and thrust belt, northern Tarim basin, NW China. Mar. Petrol. Geol. 25, 767–777. https://doi.org/10.1016/j.marpetgeo.2008.01.011.
Johannesson, K.H., Farnham, I.M., Guo, C., Stetzenbach, K.J., 1999. Rare earth element fractionation and concentration variations along a groundwater flow path within a shallow, basin-fill aquifer, southern Nevada, USA. Geochem. Cosmochim. Acta 63, 2697–2708. https://doi.org/10.1016/S0016-7037(99)00184-2.
Johannesson, K.H., Hawkins, D.L., Cortés, A., 2006. Do Archean chemical sediments record ancient seawater rare earth element patterns? Geochem. Cosmochim. Acta 70, 871–890. https://doi.org/10.1016/j.gca.2005.10.013.
Kamber, B.S., Bolhar, R., Webb, G.E., 2004. Geochemistry of late Archaean stromatolites from Zimbabwe: evidence for microbial life in restricted epicontinental seas. Precambrian Res. 132, 379–399. https://doi.org/10.1016/j.precamres.2004.03.006.
Kang, S., Datta-Gupta, A., John Lee, W., 2013. Impact of natural fractures in drainage volume calculations and optimal well placement in tight gas reservoirs. J. Petrol. Sci. Eng. 109, 206–216. https://doi.org/10.1016/j.petrol.2013.08.024.
Katz, D.A., Eberli, G.P., Swart, P.K., Smith, L.B., 2006. Tectonic-hydrothermal brecciation associated with calcite precipitation and permeability destruction in Mississippian carbonate reservoirs, Montana and Wyoming. AAPG (Am. Assoc. Pet. Geol.) Bull. 90, 1803–1841. https://doi.org/10.1306/03200605072.
Keith, M.L., Weber, J.N., 1964. Carbon and oxygen isotopic composition of selected limestones and fossils. Geochem. Cosmochim. Acta 28, 1787–1816. https://doi.org/10.1016/0016-7037(64)90022-5.
Kidder, D.L., Eddy-Dilek, C.A., 1994. Rare-earth element variation in phosphate nodules from Midcontinent Pennsylvanian cyclothems. J. Sediment. Res. 64, 584–592. https://doi.org/10.1306/D4267E15-2B26-11D7-8648000102C1865D.
Kidder, D.L., Krishnaswamy, R., Mapes, R.H., 2003. Elemental mobility in phosphatic shales during concretion growth and implications for provenance analysis. Chem. Geol. 198, 335–353. https://doi.org/10.1016/S0009-2541(03)00036-6.
Lai, J., Li, D., Ai, Y., Liu, H., Cai, D., Chen, K., Xie, Y., Wang, G., 2021. Structural diagenesis in ultra-deep tight sandstones in Kuqa depression, Tarim Basin, China. Solid Earth Discuss. 2021, 1–53. https://doi.org/10.5194/se-2021-85.
Lai, J., Wang, G., Chai, Y., Xin, Y., Wu, Q., Zhang, X., Sun, Y., 2017. Deep burial diagenesis and reservoir quality evolution of high-temperature, high-pressure sandstones: examples from Lower Cretaceous Bashijiqike Formation in Keshen area, Kuqa depression, Tarim basin of China. AAPG (Am. Assoc. Pet. Geol.) Bull. 101, 829–862. https://doi.org/10.1306/08231614008.
Lander, R.H., Laubach, S.E., 2015. Insights into rates of fracture growth and sealing from a model for quartz cementation in fractured sandstones. Geol. Soc. Am. Bull. 127, 516–538. https://doi.org/10.1130/B31092.1.
Laubach, S., Reed, R., Olson, J., Lander, R., Bonnell, L., 2004. Coevolution of crack-seal texture and fracture porosity in sedimentary rocks: cathodoluminescence observations of regional fractures. J. Struct. Geol. 26, 967–982. https://doi.org/10.1016/j.jsg.2003.08.019.
Laubach, S.E., 2003. Practical approaches to identifying sealed and open fractures. AAPG (Am. Assoc. Pet. Geol.) Bull. 87, 561–579. https://doi.org/10.1306/11060201106.
Laubach, S.E., 1988. Subsurface fractures and their relationship to stress history in East Texas basin sandstone. Tectonophysics 156, 37–49. https://doi.org/10.1016/0040-1951(88)90281-8.
Laubach, S.E., Lander, R.H., Criscenti, L.J., Anovitz, L.M., Urai, J.L., Pollyea, R.M., Hooker, J.N., Narr, W., Evans, M.A., Kerisit, S.N., Olson, J.E., Dewers, T., Fisher, D., Bodnar, R., Evans, B., Dove, P., Bonnell, L.M., Marder, M.P., Pyrak-Nolte, L., 2019. The role of chemistry in fracture pattern development and opportunities to Advance interpretations of geological materials. Rev. Geophys. 57, 1065–1111. https://doi.org/10.1029/2019RG000671.
Lavenu, A.P.C., Lamarche, J., Gallois, A., Gauthier, B.D.M., 2013. Tectonic versus diagenetic origin of fractures in a naturally fractured carbonate reservoir analog (Nerthe anticline, southeastern France). AAPG (Am. Assoc. Pet. Geol.) Bull. 97, 2207–2232. https://doi.org/10.1306/04041312225.
Lawrence, M.G., Greig, A., Collerson, K.D., Kamber, B.S., 2006. Rare earth element and yttrium variability in South east Queensland waterways. Aquat. Geochem. 12, 39–72. https://doi.org/10.1007/s10498-005-4471-8.
Lee, M.R., Martin, R.W., Trager-Cowan, C., Edwards, P.R., 2005. Imaging of cathodoluminescence zoning in calcite by Scanning electron microscopy and hyperspectral mapping. J. Sediment. Res. 75, 313–322, 20121219164439.
Lee, Y.-J., Morse, J.W., 1999. Calcite precipitation in synthetic veins: implications for the time and fluid volume necessary for vein filling. Chem. Geol. 156, 151–170. https://doi.org/10.1016/S0009-2541(98)00183-1.
Lee, Y.-J., Wiltschko, D.V., Grossman, E.L., Morse, J.W., Lamb, W.M., 1997. Sequential vein growth with fault displacement: an example from the Austin Chalk Formation, Texas. J. Geophys. Res. Solid Earth 102, 22611–22628. https://doi.org/10.1029/97JB01945.
Li, H., Tang, H., Qin, Q., Zhou, J., Qin, Z., Fan, C., Su, P., Wang, Q., Zhong, C., 2019. Characteristics, formation periods and genetic mechanisms of tectonic fractures in the tight gas sandstones reservoir: a case study of Xujiahe Formation in YB area, Sichuan Basin, China. J. Petrol. Sci. Eng. 178, 723–735. https://doi.org/10.1016/j.petrol.2019.04.007.
Li, X., Gao, Z., Li, S., Feng, J., Zhao, X., Guo, M., 2013. Relationship between Conglomeratic characteristics and tectonic evolution of upper Jurassic-lower Cretaceous in Kuqa foreland basin. Acta Sedimentol. Sin. 31, 980–993.
Li, Z., Song, W., Peng, S., Wang, D., Zhang, Z., 2004. Mesozoic–Cenozoic tectonic relationships between the Kuqa subbasin and Tian Shan, northwest China: constraints from depositional records. Sediment. Geol. 172, 223–249. https://doi.org/10.1016/j.sedgeo.2004.09.002.
Liu, C., Rong, H., Chen, S., Jia, J., Tang, Y., Deng, Y., 2021. Occurrence, mineralogy and geochemistry of fracture fillings in tight sandstone and their constraints on multiple-stage diagenetic fluids and reservoir quality: an example from the Kuqa foreland thrust belt, Tarim Basin, China. J. Petrol. Sci. Eng. 201, 108409 https://doi.org/10.1016/j.petrol.2021.108409.
Liu, C., Zhang, H., Han, B., Zhang, R., Chen, G., 2009. Reservoir characteristics and control factors of deep-burial clastic rocks in Dabei zone of Kuche Sag. Nat. Gas Geosci. 20, 504–512.
Liu, L., Huang, J., Wang, C., Huang, K., Tong, H., Zhong, Q., 2010. Cathodoluminescence zonal texture of calcite cement in carbonate rock and its relationship with trace element composition: a case of Ordovician carbonate rock of Tahe Oilfield, Tarim Basin. Mar. Origin Petrol. Geol. 15, 55–60.
Liu, L., Zhou, H., Zhang, C., Yan, B., Yang, F., Qu, Y., 2022. Synergistic deformation mechanisms and basin-mountain coupling of Kelasu structural belt in Kuqa Depression. Chin. J. Geol. 57, 61–72.

Liu, Y., Hu, Z., Gao, S., Günther, D., Xu, J., Gao, C., Chen, H., 2008. In situ analysis of major and trace elements of anhydrous minerals by LA-ICP-MS without applying an internal standard. Chem. Geol. 257, 34–43. https://doi.org/10.1016/j.chemgeo.2008.08.004.

Lu, H., David, G.H., Jia, D., Cai, D., Wu, S., Chen, C., Zenon, C.V., Shi, Y., 1994. Rejuvenation of the Kuqa foreland basin, northern flank of the Tarim Basin, northwest China. Int. Geol. Rev. 36, 1151–1158. https://doi.org/10.1080/00206819409465509.

Lyu, W., Zeng, L., Zhang, B., Miao, F., Lyu, P., Dong, S., 2017. Influence of natural fractures on gas accumulation in the Upper Triassic tight gas sandstones in the northwestern Sichuan Basin, China. Mar. Petrol. Geol. 83, 60–72. https://doi.org/10.1016/j.marpetgeo.2017.03.004.

Ma, Y., Zhang, R., Tang, Y., Chen, J., Mo, T., Wang, J., Xie, P., 2016. Lithofacies Paleogeography of Cretaceous Bashijiqike Formation in Kuqa depression,Tarim Basin. Xinjing Pet. Geol. 37, 249–256. https://doi.org/10.7657/XJPG20160301.

Machel, H.G., 2000. Application of cathodoluminescence to carbonate diagenesis. In: Pagel, M., Barbin, V., Blanc, P., Ohnenstetter, D. (Eds.), Cathodoluminescence in Geosciences. Springer Berlin Heidelberg, Berlin, Heidelberg, pp. 271–301. https://doi.org/10.1007/978-3-662-04086-7_11.

Machel, H.G., Mason, R.A., Mariano, A.N., Mucci, A., 1991. Causes and emission of luminescence in calcite and dolomite. In: Barker, C.E., Burruss, R.C., Kopp, O.C., Machel, H.G., Marshall, D.J., Wright, P., Colbum, H.Y. (Eds.), Luminescence Microscopy and Spectroscopy: Qualitative and Quantitative Applications, vol. 0. SEPM Society for Sedimentary Geology. https://doi.org/10.2110/scn.91.25.0009.

Mangenot, X., Bonifacie, M., Gasparrini, M., Götz, A., Chaduteau, C., Ader, M., Rouchon, V., 2017. Coupling Δ47 and fluid inclusion thermometry on carbonate cements to precisely reconstruct the temperature, salinity and δ18O of paleo-groundwater in sedimentary basins. Chem. Geol. 472, 44–57. https://doi.org/10.1016/j.chemgeo.2017.10.011.

Marquez, X.M., Mountjoy, E.W., 1996. Microfractures due to overpressures caused by thermal cracking in well-sealed Upper Devonian reservoirs, deep Alberta Basin. AAPG (Am. Assoc. Pet. Geol.) Bull. 80, 570–588.

Maskenskaya, O.M., Drake, H., Broman, C., Hogmalm, J.K., Czuppon, G., Åström, M.E., 2014. Source and character of syntaxial hydrothermal calcite veins in Paleoproterozoic crystalline rocks revealed by fine-scale investigations. Geofluids 14, 495–511. https://doi.org/10.1111/gfl.12092.

McLennan, S.M., 2001. Relationships between the trace element composition of sedimentary rocks and upper continental crust. G-cubed 2. https://doi.org/10.1029/2000GC000109.

Montanez, I.P., 1994. Late diagenetic dolomitization of Lower Ordovician, Upper Knox carbonates: a record of the hydrodynamic evolution of the southern Appalachian Basin. AAPG (Am. Assoc. Pet. Geol.) Bull. 78, 1210–1239.

Morad, S., Worden, R.H., Ketzer, J.M., 1999. Oxygen and hydrogen isotopic composition of diagenetic clay minerals in sandstones: a review of the data and controls. In: Clay Mineral Cements in Sandstones. John Wiley & Sons, Ltd, pp. 63–91. https://doi.org/10.1002/9781444304336.ch3.

Nozaki, Y., Lerche, D., Alibo, D.S., Tsutsumi, M., 2000. Dissolved indium and rare earth elements in three Japanese rivers and Tokyo Bay: evidence for anthropogenic Gd and in. Geochem. Cosmochim. Acta 64, 3975–3982. https://doi.org/10.1016/S0016-7037(00)00472-5.

Nozaki, Y., Zhang, J., Amakawa, H., 1997. The fractionation between Y and Ho in the marine environment. Earth Planet Sci. Lett. 148, 329–340. https://doi.org/10.1016/S0012-821X(97)00034-4.

Pagel, M., Barbin, V., Blanc, P., Ohnenstetter, D., 2000. Cathodoluminescence in geosciences: an introduction. In: Cathodoluminescence in Geosciences. Springer, pp. 1–21.

Passchier, C.W., 1996. Microtectonics. Springer Verlag, Berlin.

Ramsay, J.G., 1983. The Techniques of Modern Structural Geology. Academic Press, London.

Reed, R.M., Milliken, K.L., 2003. How to overcome imaging problems associated with carbonate minerals on SEM-based cathodoluminescence systems. J. Sediment. Res. 73, 328–332. https://doi.org/10.1306/081002730328.

Richter, D.K., Götte, Th, Götze, J., Neuser, R.D., 2003. Progress in application of cathodoluminescence (CL) in sedimentary petrology. Mineral. Petrol. 79, 127–166. https://doi.org/10.1007/s00710-003-0237-4.

Rimsa, A., Whitehouse, M.J., Johansson, L., Piazolo, S., 2007. Brittle fracturing and fracture healing of zircon: an integrated cathodoluminescence, EBSD, U-Th-Pb, and REE study. Am. Mineral. 92, 1213–1224. https://doi.org/10.2138/am.2007.2458.

Rollinson, H.R., 1993. Using Geochemical Data: Evaluation, Presentation, Interpretation, first ed. Routledge. https://doi.org/10.4324/9781315845548. 0.

Rye, D.M., Bradbury, H.J., 1988. Fluid flow in the crust; an example from a Pyrenean thrust ramp. Am. J. Sci. 288, 197–235. https://doi.org/10.2475/ajs.288.3.197.

Shen, Z., Gong, Y., Liu, S., Lv, Z., 2010. A discussion on genesis of the upper Triassic Xujiahe formation water in Xinchang area, western Sichuan depression. Geol. Rev. 56, 82–88.

Shi, C., Zhang, H., Zhou, S., Wang, Zuotao, Jiang, J., Zhang, X., Zuo, X., Lou, H., Wang, Zhenhong, Chen, C., 2020. Comparative study on deep and high yielding reservoir characteristics and controlling factors of Cretaceous Bashijiqike Formation in Kelasu structural belt and Qiulitage structural belt of Kuqa Depression , Tarim Basin. Nat. Gas Geosci. 31, 1126–1138.

Shields, G.A., Webb, G.E., 2004. Has the REE composition of seawater changed over geological time? Chem. Geol. 204 (1–2), 103–107.

Sholkovitz, E.R., Piepgras, D.J., Jacobsen, S.B., 1989. The pore water chemistry of rare earth elements in Buzzards Bay sediments. Geochem. Cosmochim. Acta 53, 2847–2856. https://doi.org/10.1016/0016-7037(89)90162-2.

Smith, A.P., Fischer, M.P., Evans, M.A., 2014. On the homogeneity of fluids forming bedding-parallel veins. Geofluids 14, 45–57. https://doi.org/10.1111/gfl.12040.

Solano, N., Zambrano, L., Aguilera, R., 2011. Cumulative-Gas-production distribution on the nikanassin tight gas formation, Alberta and British Columbia, Canada. SPE Reservoir Eval. Eng. 14, 357–376. https://doi.org/10.2118/132923-PA.

Sprunt, E.S., Nur, A., 1979. Microcracking and healing in granites: new evidence from cathodoluminescence. Science 205, 495–497. https://doi.org/10.1126/science.205.4405.495.

Steven, D.H., Campbell, S.N., Peter, J.J.K., 2003. Modification of fracture porosity by multiphase vein mineralization in an Oligocene nontropical carbonate reservoir, Taranaki Basin, New Zealand. AAPG (Am. Assoc. Pet. Geol.) Bull. 87, 1575–1597. https://doi.org/10.1306/06040301103.

Sverjensky, D.A., 1984. Europium redox equilibria in aqueous solution. Earth Planet Sci. Lett. 67, 70–78. https://doi.org/10.1016/0012-821X(84)90039-6.

Travé, A., Calvet, F., Soler, A., Labaume, P., 1998. Fracturing and fluid migration during Palaeogene compression and Neogene extension in the Catalan coastal ranges, Spain. Sedimentology 45, 1063–1082. https://doi.org/10.1046/j.1365-3091.1998.00191.x.

Ukar, E., Laubach, S.E., 2016. Syn- and postkinematic cement textures in fractured carbonate rocks: insights from advanced cathodoluminescence imaging. Tectonophysics 690, 190–205. https://doi.org/10.1016/j.tecto.2016.05.001.

Van Kranendonk, M.J., Webb, G.E., Kamber, B.S., 2003. Geological and trace element evidence for a marine sedimentary environment of deposition and biogenicity of 3.45 Ga stromatolitic carbonates in the Pilbara Craton, and support for a reducing Archaean ocean. Geobiology 1, 91–108. https://doi.org/10.1046/j.1472-4669.2003.00014.x.

Veras, J.D., de Souza Neto, J.A., Sial, A.N., Ferreira, V.P., Neumann, V.H., 2021. Stable isotope and chemical stratigraphy of the eocene Tambaba formation: correlations with the Paleocene–eocene thermal maximum event. Geol. Soc. London Special Publ. 507, 273–291. https://doi.org/10.1144/SP507-2020-35.

Wang, K., Zhang, R., Wang, J., Sun, X., Yang, X., 2021. Distribution and origin of tectonic fractures in ultra-deep tight sandstone reservoirs: a case study of Keshen gas field , Kuqa foreland thrust belt , Tarim Basin. Oil Gas Geol. 42, 338–353.

Wogelius, R.A., Fraser, D.G., Wall, G.R.T., Grime, G.W., 1997. Trace element and isotopic zonation in vein calcite from the Mendip Hills, UK, with spatial-process correlation analysis. Geochem. Cosmochim. Acta 61, 2037–2051. https://doi.org/10.1016/S0016-7037(97)00065-3.

Xi, K., Cao, Y., Lin, M., Liu, K., Wu, S., Yuan, G., Yang, T., 2019. Applications of light stable isotopes (C, O, H) in the study of sandstone diagenesis: a review. Acta Geol. Sin. English Ed. 93, 213–226. https://doi.org/10.1111/1755-6724.13769.

Yardley, B.W.D., 2013. The chemical composition of Metasomatic fluids in the crust. In: Metasomatism and the Chemical Transformation of Rock: the Role of Fluids in Terrestrial and Extraterrestrial Processes. Springer Berlin Heidelberg, Berlin, Heidelberg, pp. 17–51. https://doi.org/10.1007/978-3-642-28394-9_2.

Yin, A., Nie, S., Craig, P., Harrison, T.M., Ryerson, F.J., Xianglin, Q., Geng, Y., 1998. Late Cenozoic tectonic evolution of the southern Chinese Tian Shan. Tectonics 17, 1–27. https://doi.org/10.1029/97TC03140.

Yu, X., Hou, G., Neng, Y., Li, J., Wei, H., 2016. Development and distribution characteristics of tectonic fractures in Kuqa depression. Geol. J. China Univ. 22, 644–656.

Yuan, J., Yang, X., Yuan, L., Cheng, R., Zhu, Z., Li, T., Dong, D., 2015. Cementation and its relationship with tectonic fractures of Cretaceous sandstones in DB gas field of Kuqa sub-basin. Acta Sedimentol. Sin. 33, 754–763.

Zeng, L., Wang, H., Gong, L., Liu, B., 2010. Impacts of the tectonic stress field on natural gas migration and accumulation: a case study of the Kuqa Depression in the Tarim Basin, China. Mar. Petrol. Geol. 27, 1616–1627. https://doi.org/10.1016/j.marpetgeo.2010.04.010.

Zhang, Y., Han, D., Yang, C., Yuan, R., Wang, C., Zhang, J., 2020. Migration law of fracture filling fluid in ultra-deep clastic reservoirs: a case study of the Cretaceous Bashijiqike Formation in Keshen well block , Kuqa depression. Acta Pet. Sin. 41, 292–300.

Zhao, Y., Li, S., Li, D., Guo, L., Dai, L., Tao, J., 2019. Rare earth element geochemistry of carbonate and its paleoenvironmental implications. Geotect. Metallogenia 43, 141–167. https://doi.org/10.16539/j.ddgzyckx.2019.01.011.

Zou, Y.R., Zhao, C., Wang, Y., Zhao, W., Peng, P., Shuai, Y., 2006. Characteristics and origin of natural gases in the Kuqa depression of Tarim Basin, NW China. Org. Geochem. 37, 280–290. https://doi.org/10.1016/j.orggeochem.2005.11.002.